remote sensing

Supplementary figures

Evapotranspiration Changes over the European Alps: Consistency of Trends and Their Drivers between the MOD16 and SSEBop Algorithms

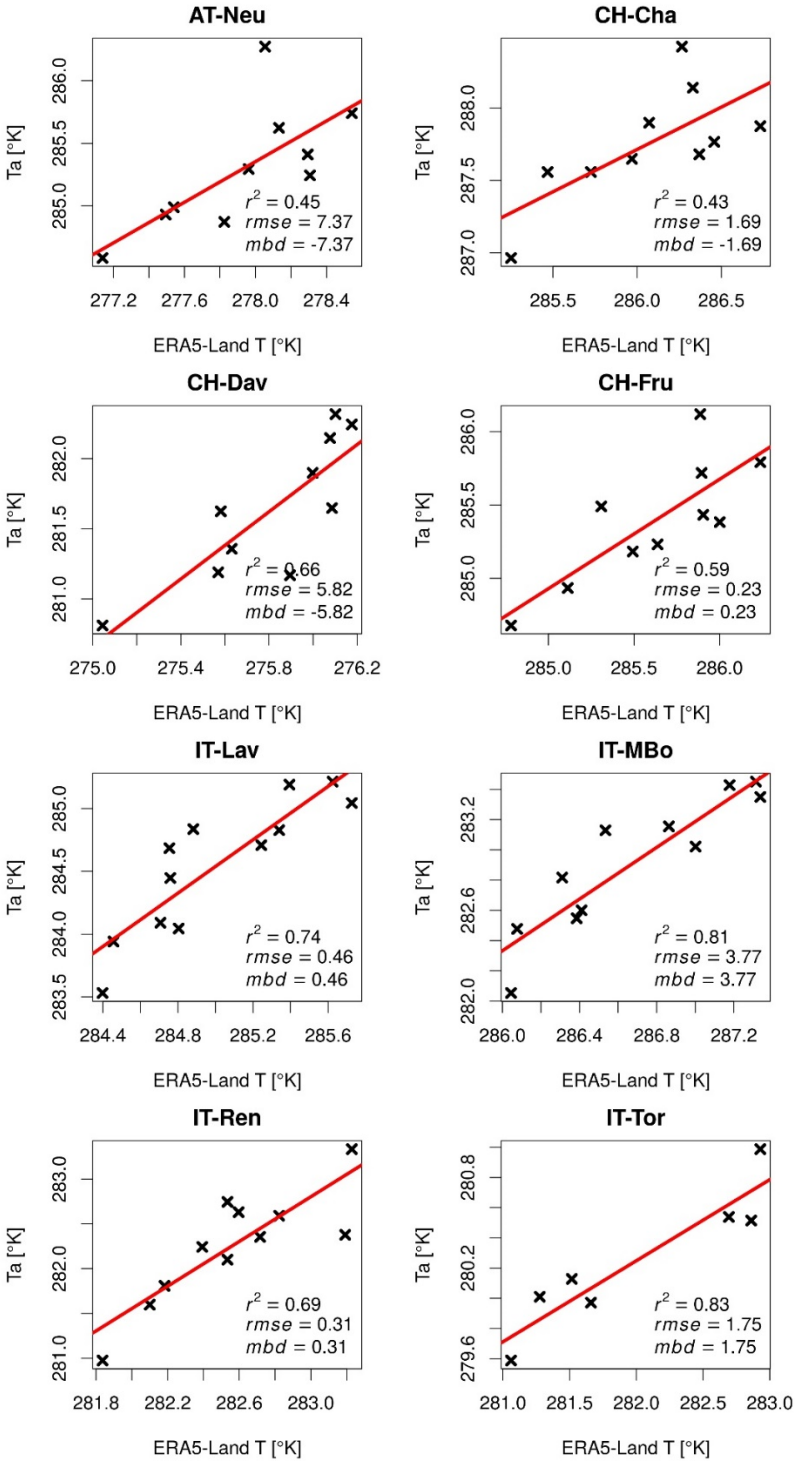

Figure S1. Correlation between growing season average air temperature measured at eddy flux towers sites and extracted from ERA5 Land reanalysis at the location of the tower sites.

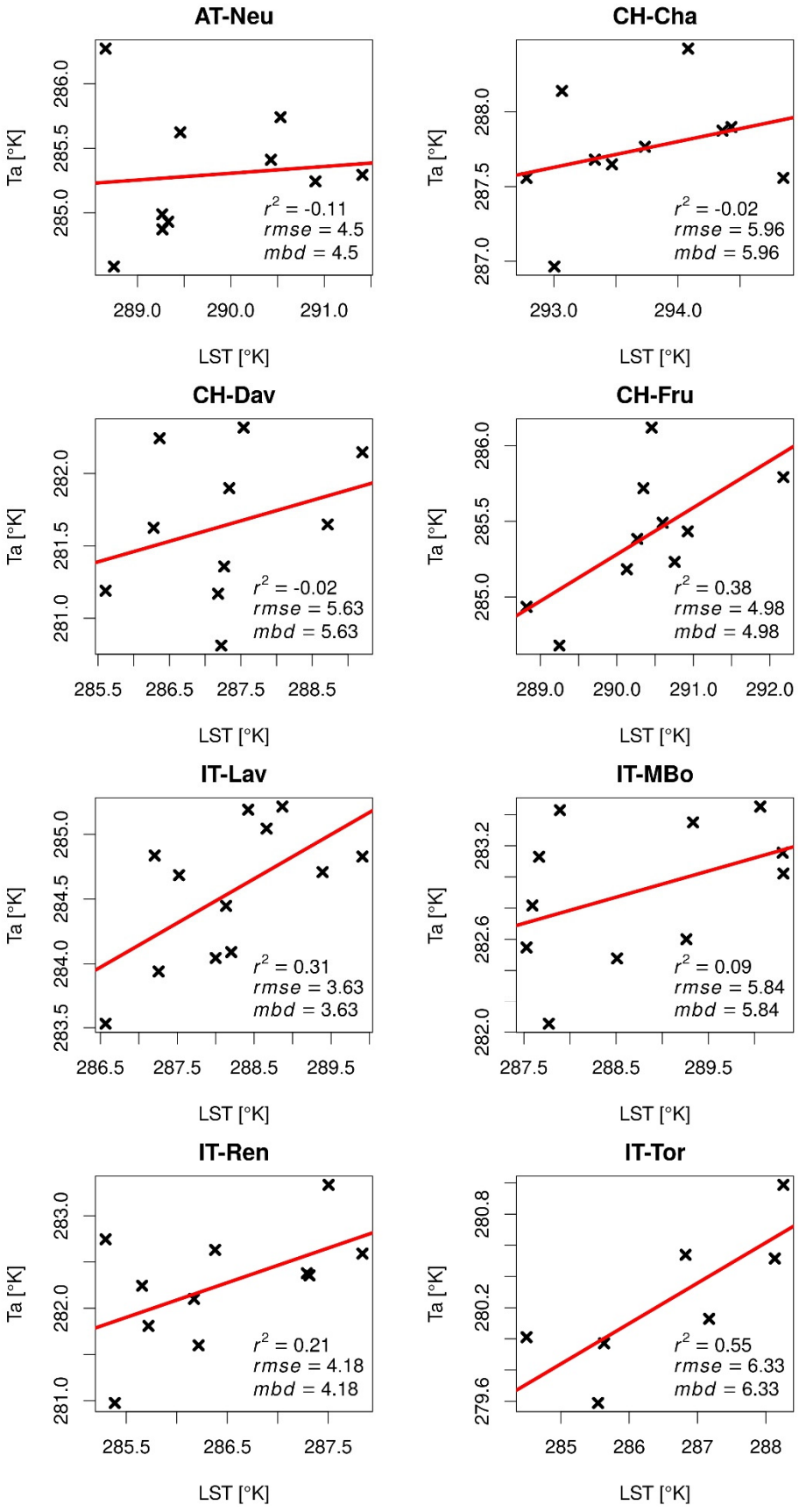

Figure S2. Correlation between growing season average air temperature measured at eddy flux towers sites and growing season average LST extracted from the MOD11 product at the location of the tower sites.

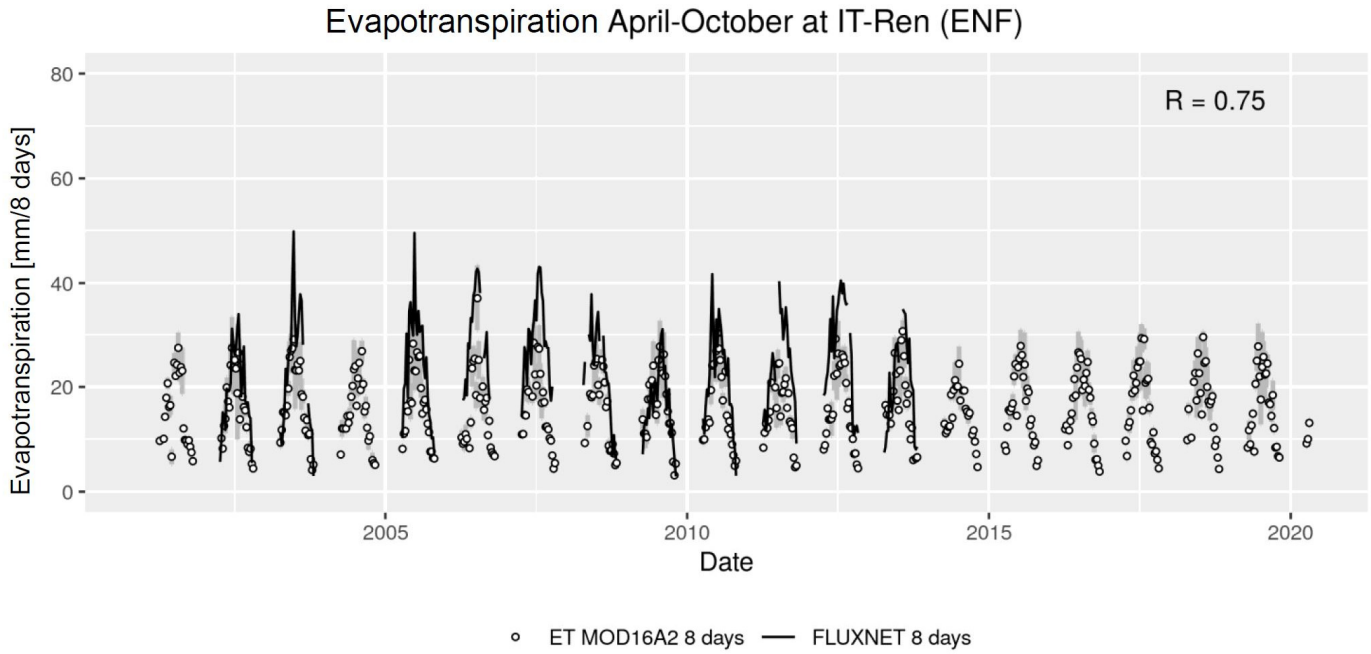

Figure S3. Timeseries of ET from eddy covariance measurements and from the MOD16 product at the Fluxnet site IT-Ren.

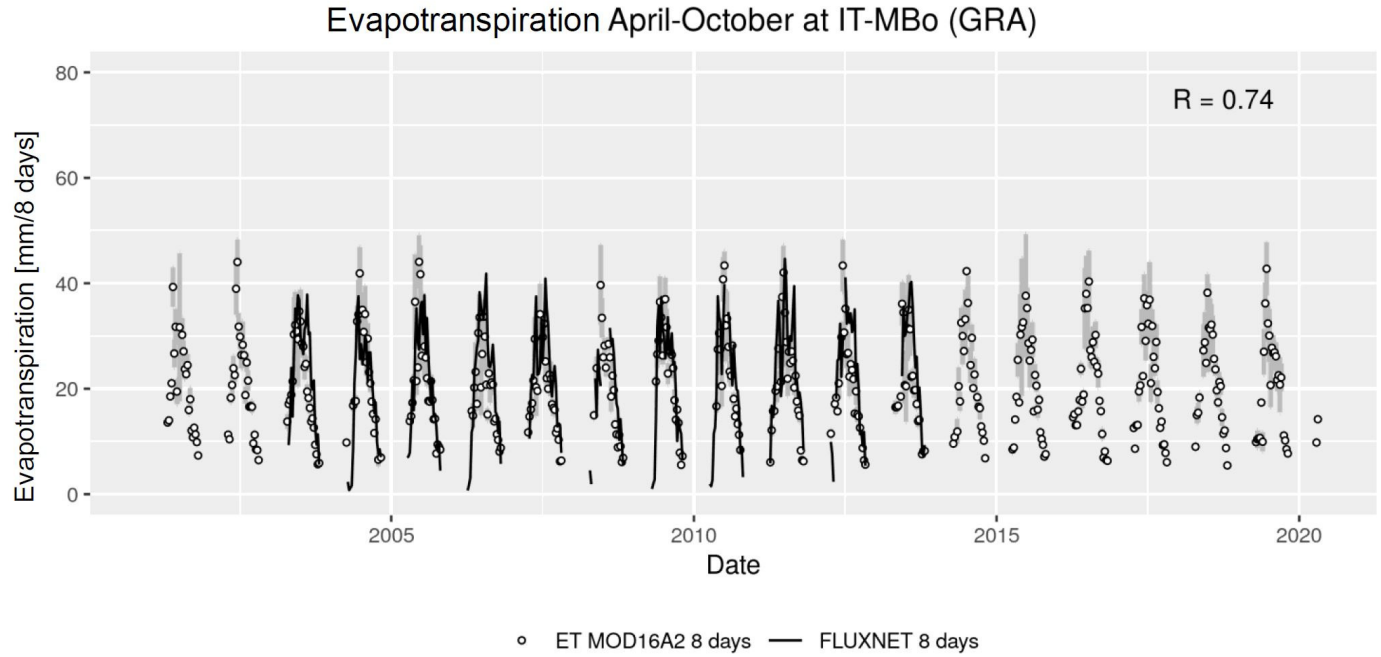

Figure S4. Timeseries of ET from eddy covariance measurements and from the MOD16 product at the Fluxnet site IT-MBo.

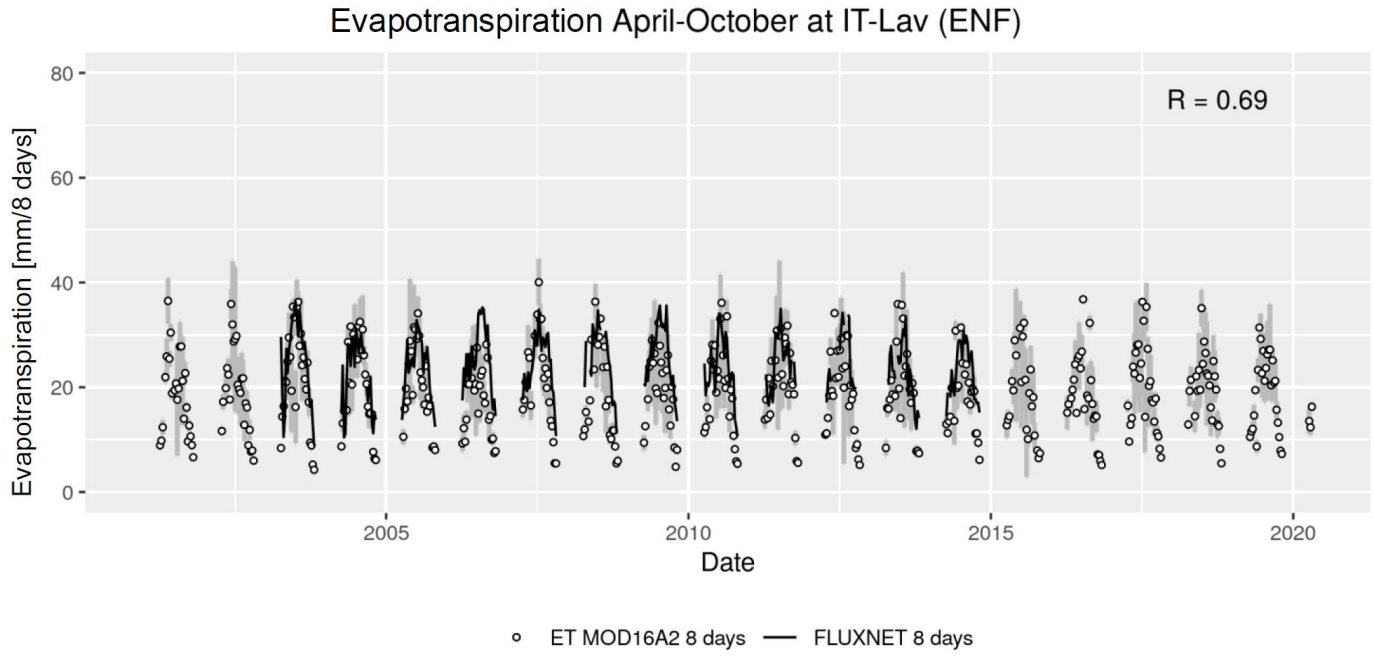

Figure S5. Timeseries of ET from eddy covariance measurements and from the MOD16 product at the Fluxnet site IT-LAV.

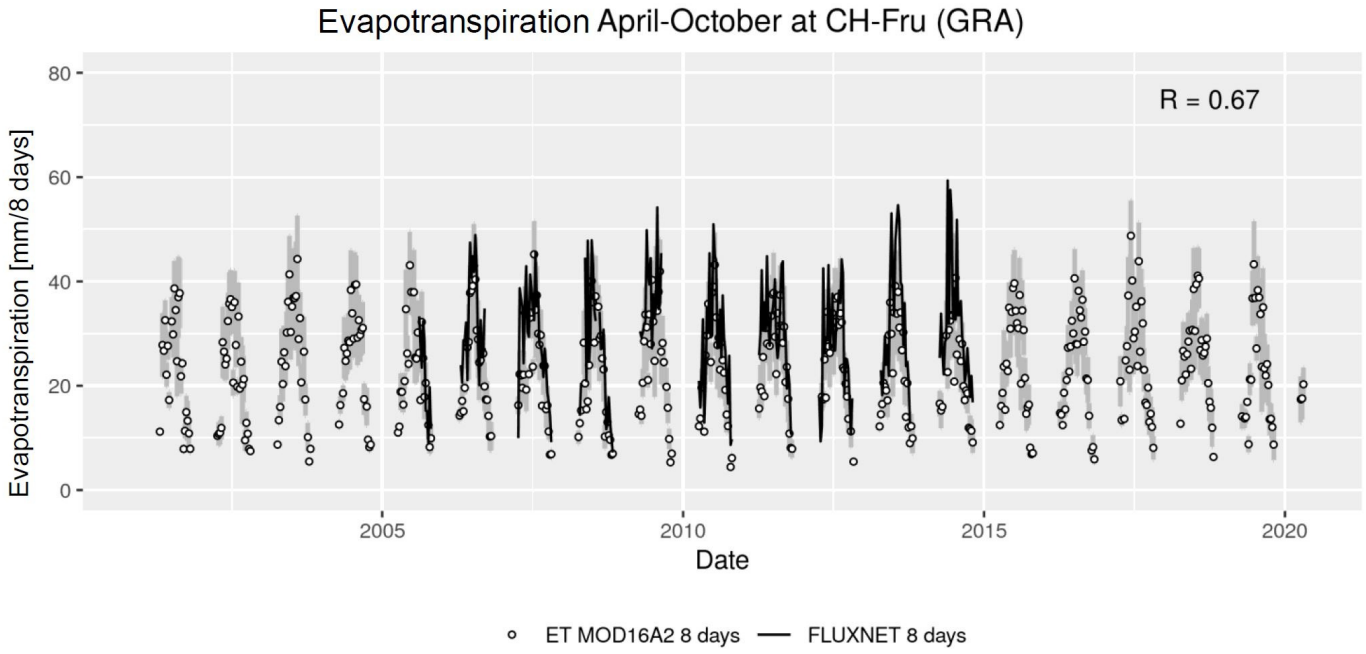

Figure S6. Timeseries of ET from eddy covariance measurements and from the MOD16 product at the Fluxnet site CH-Fru.

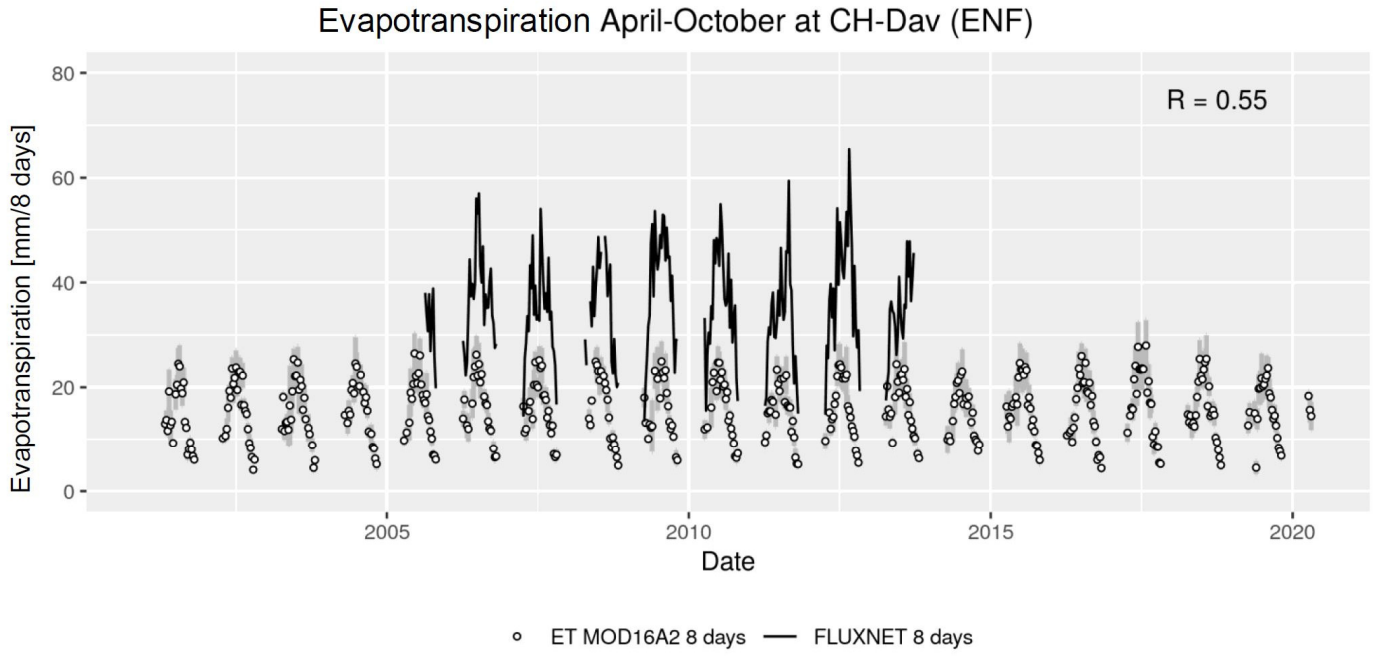

Figure S7. Timeseries of ET from eddy covariance measurements and from the MOD16 product at the Fluxnet site CH_Dav.

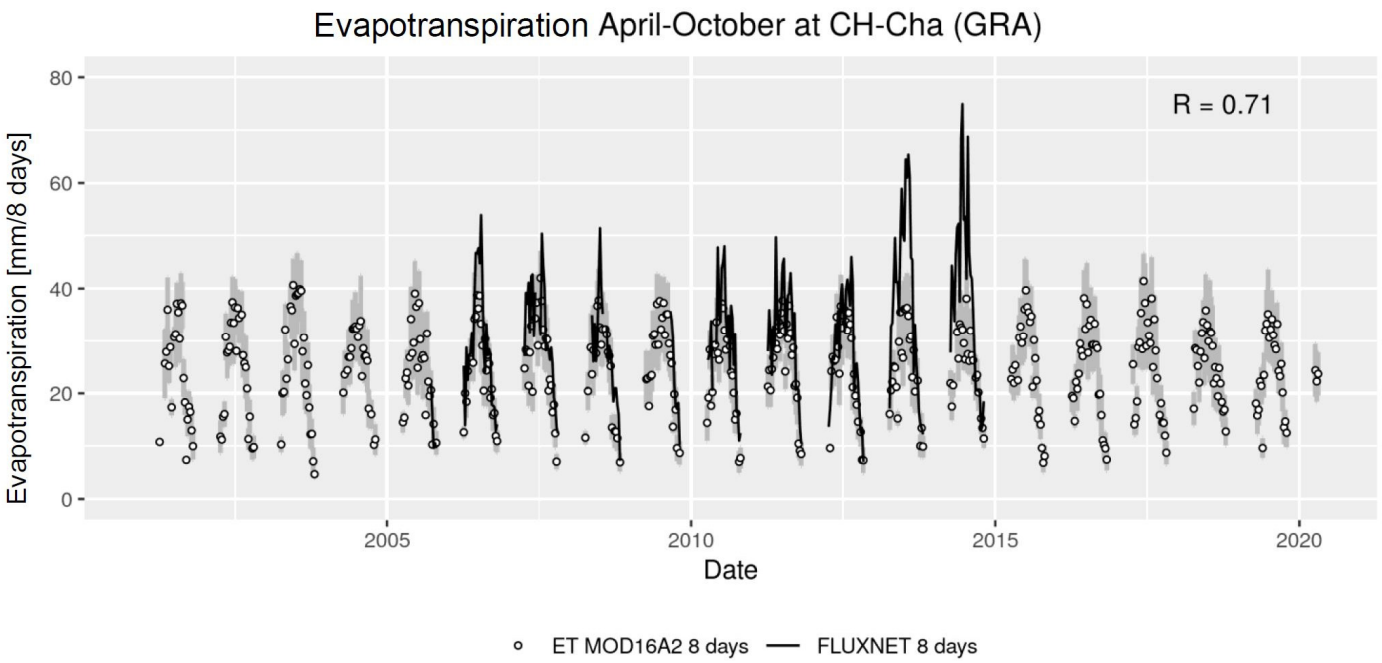

Figure S8. Timeseries of ET from eddy covariance measurements and from the MOD16 product at the Fluxnet site CH_Cha.

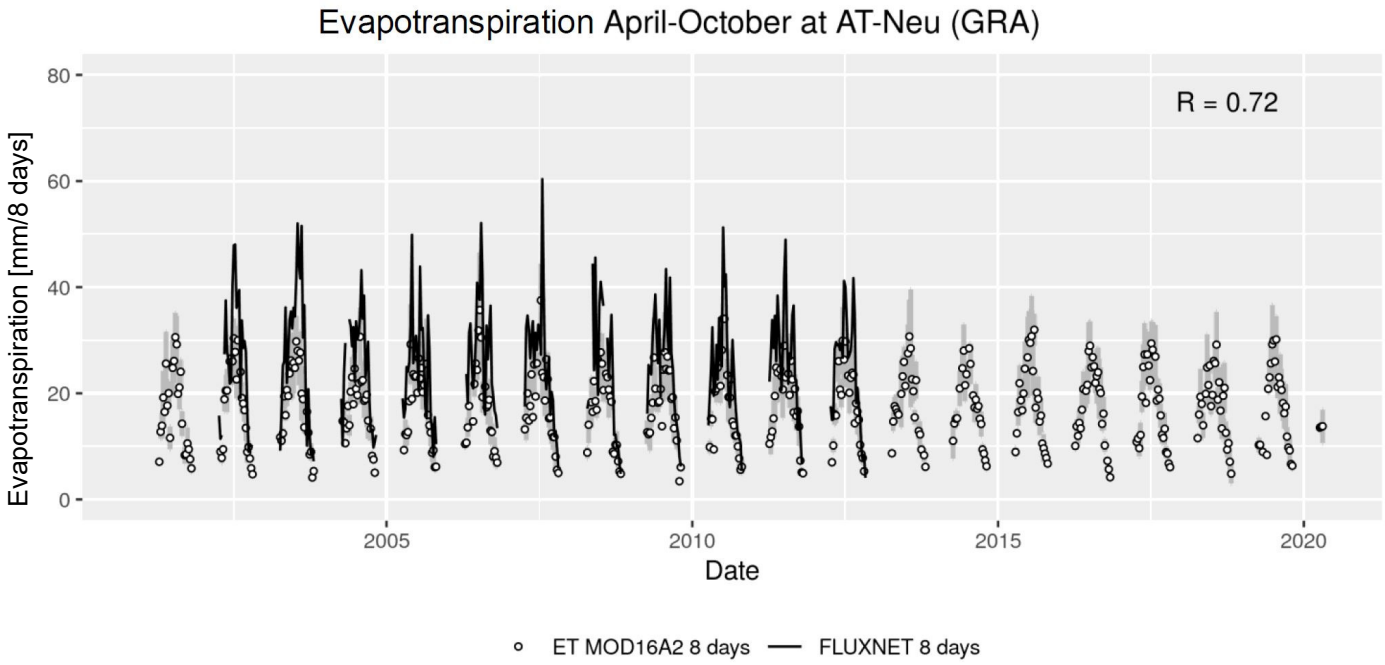

Figure S9. Timeseries of ET from eddy covariance measurements and from the MOD16 product at the Fluxnet site AT_Neu.

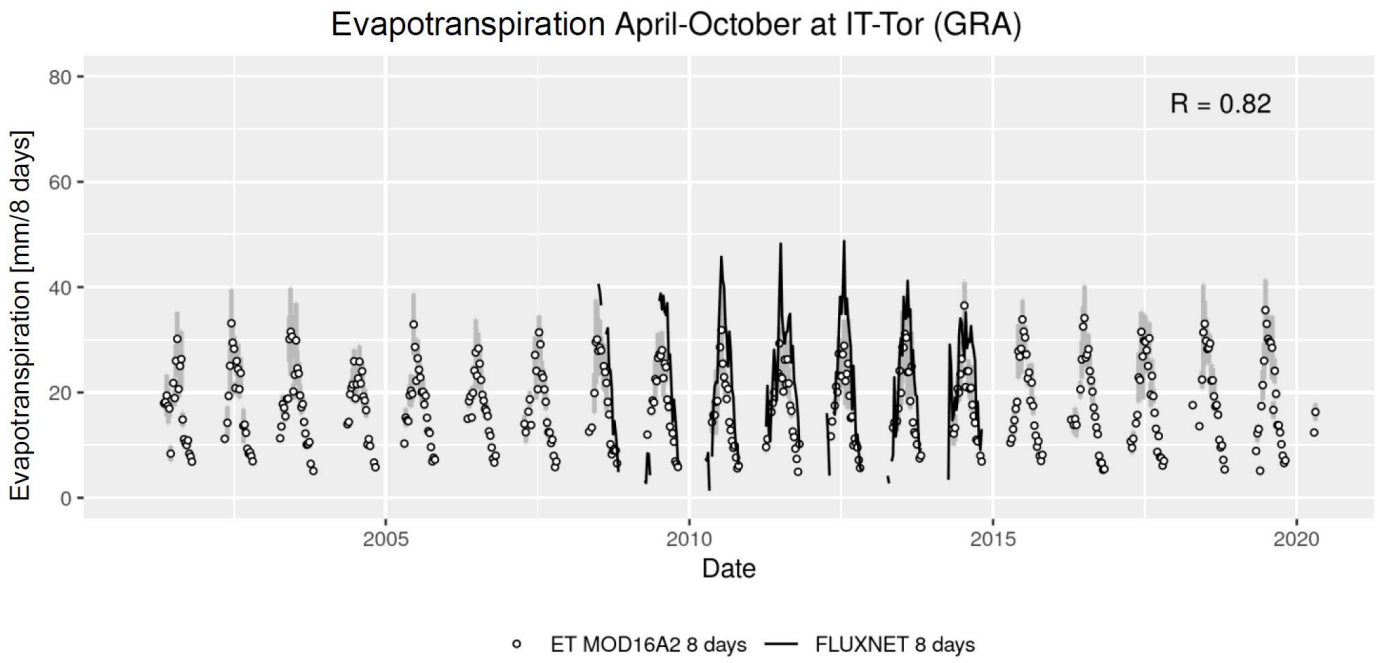

Figure S10. Timeseries of ET from eddy covariance measurements and from the MOD16 product at the Fluxnet site IT-Tor.

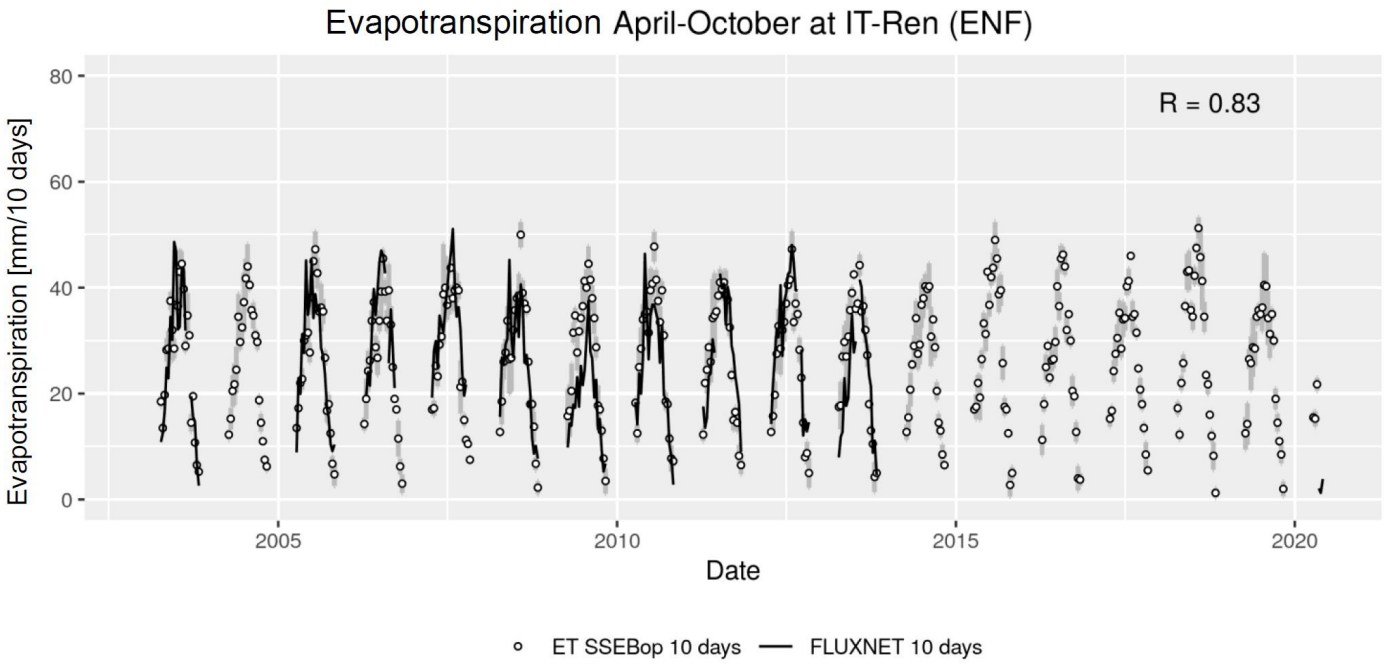

Figure S11. Timeseries of ET from eddy covariance measurements and from the SSEBop product at the Fluxnet site IT-Ren.

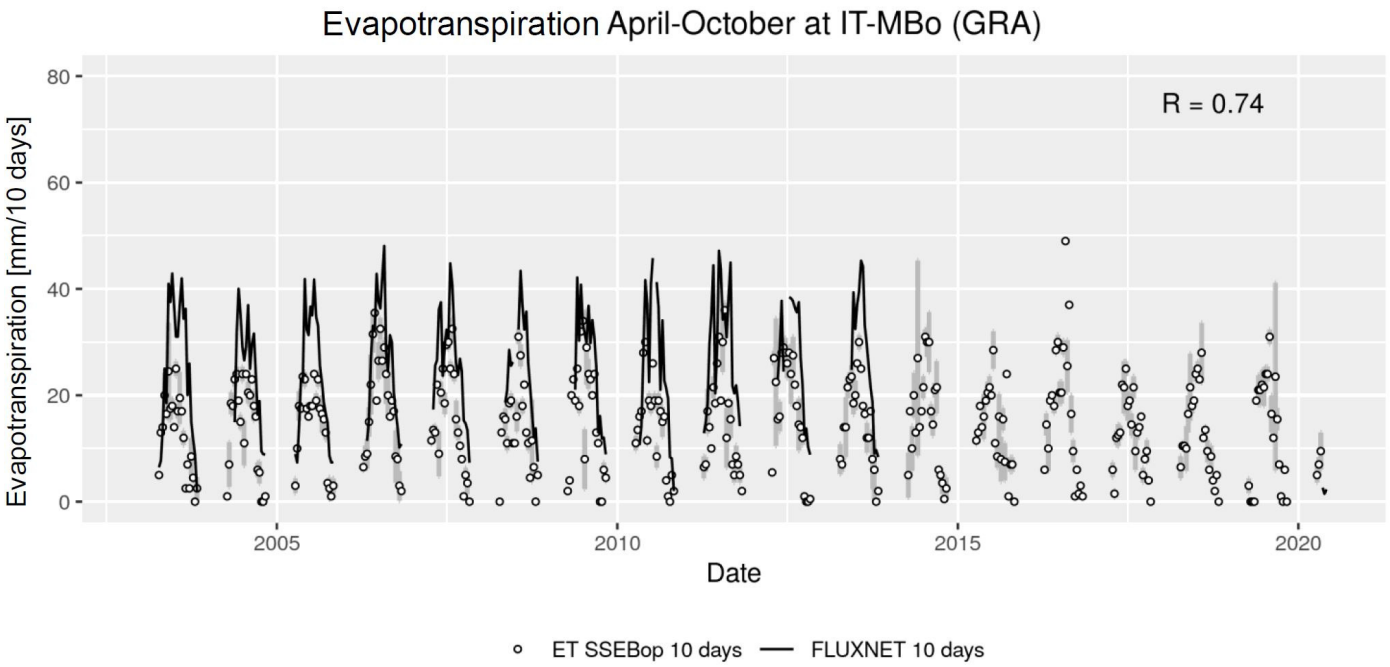

Figure S12. Timeseries of ET from eddy covariance measurements and from the SSEBop product at the Fluxnet site IT-MBo.

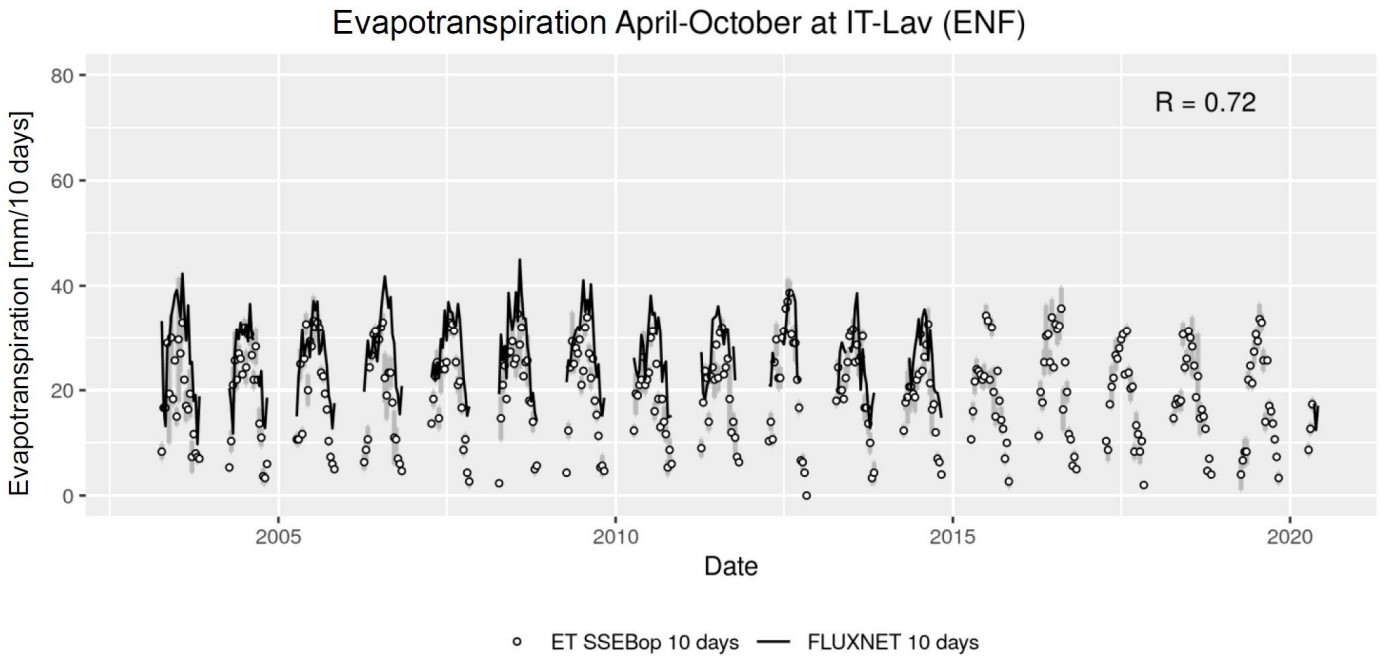

Figure S13. Timeseries of ET from eddy covariance measurements and from the SSEBop product at the Fluxnet site IT-Lav.

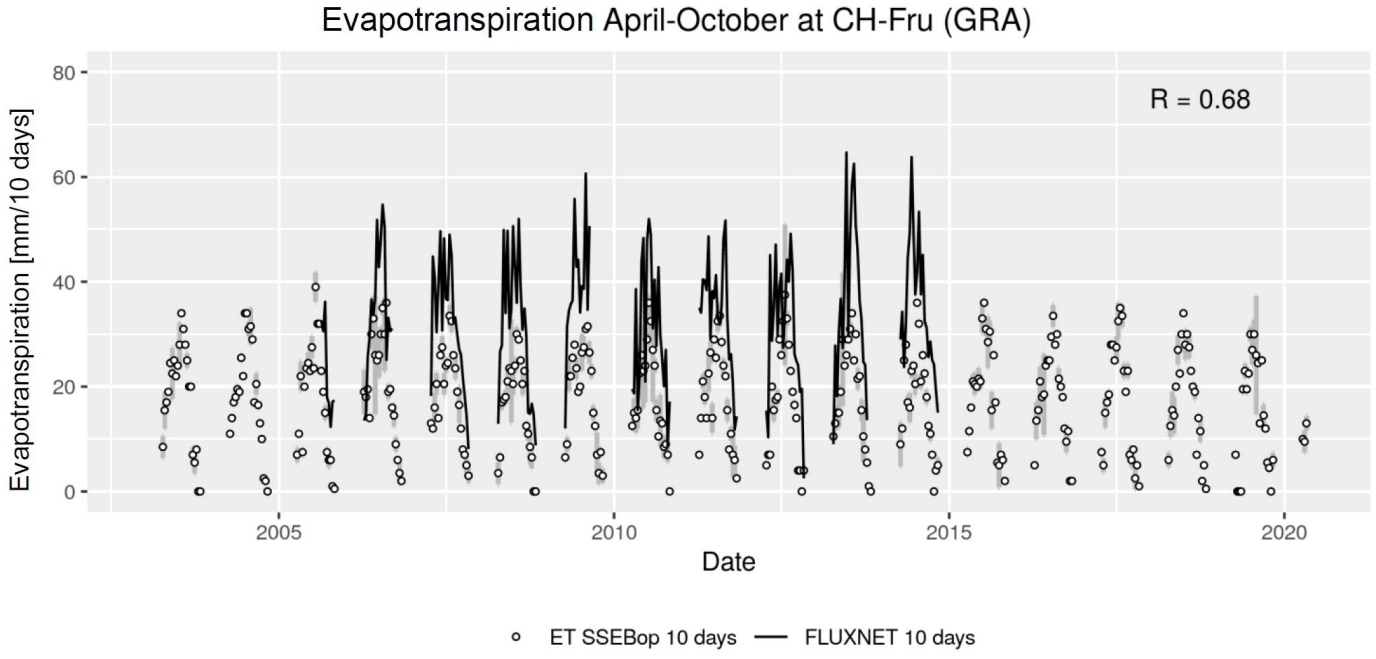

Figure S14. Timeseries of ET from eddy covariance measurements and from the SSEBop product at the Fluxnet site CH_Fru.

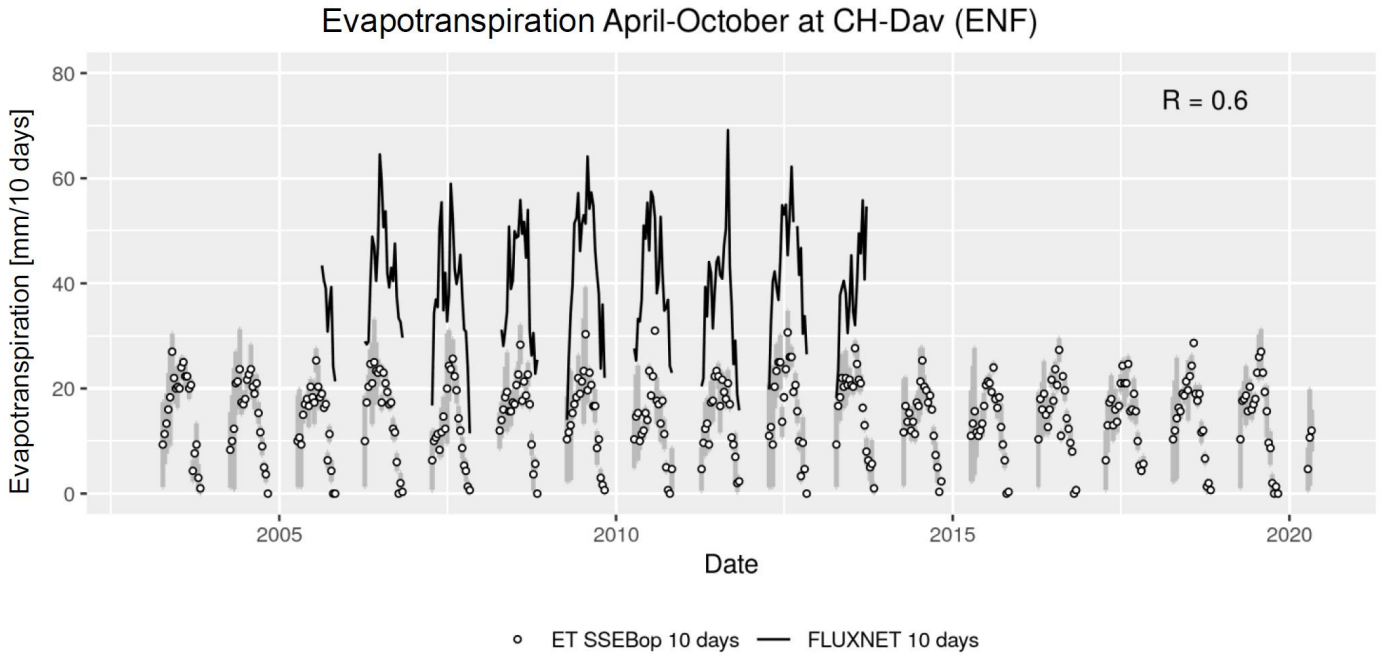

Figure S15. Timeseries of ET from eddy covariance measurements and from the SSEBop product at the Fluxnet site CH_Dav.

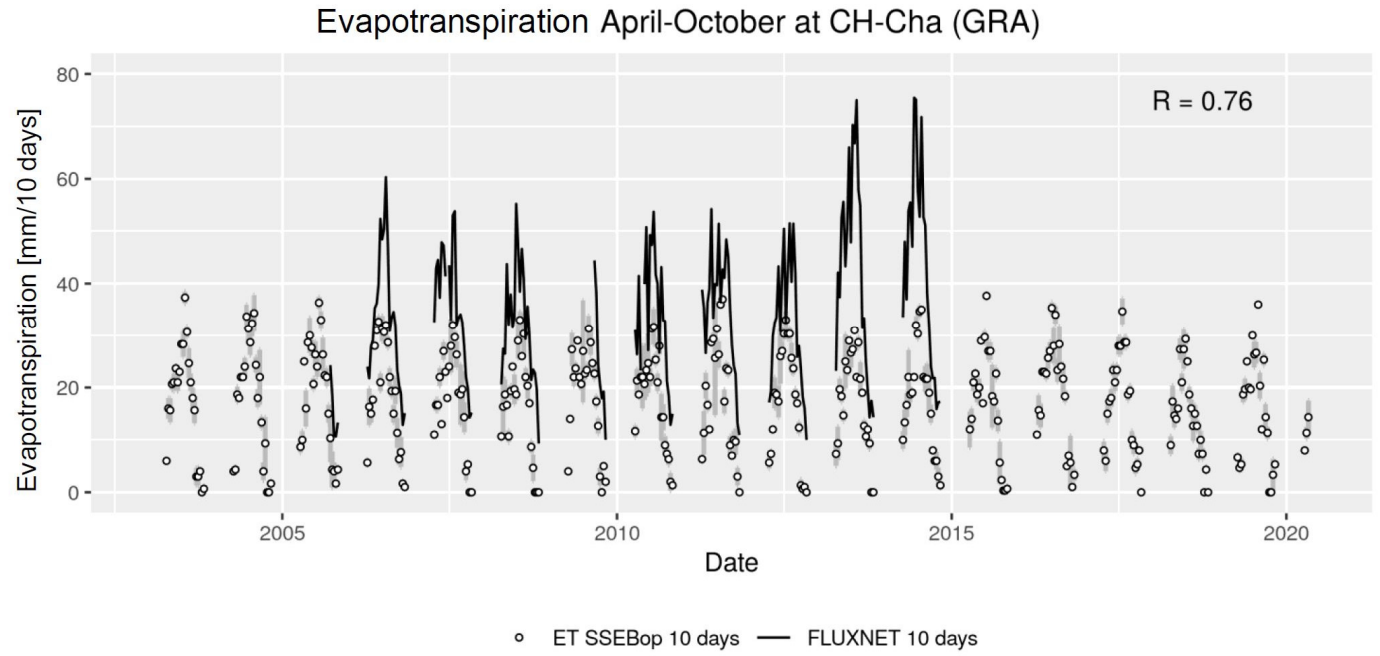

Figure S16. Timeseries of ET from eddy covariance measurements and from the SSEBop product at the Fluxnet site CH-Cha.

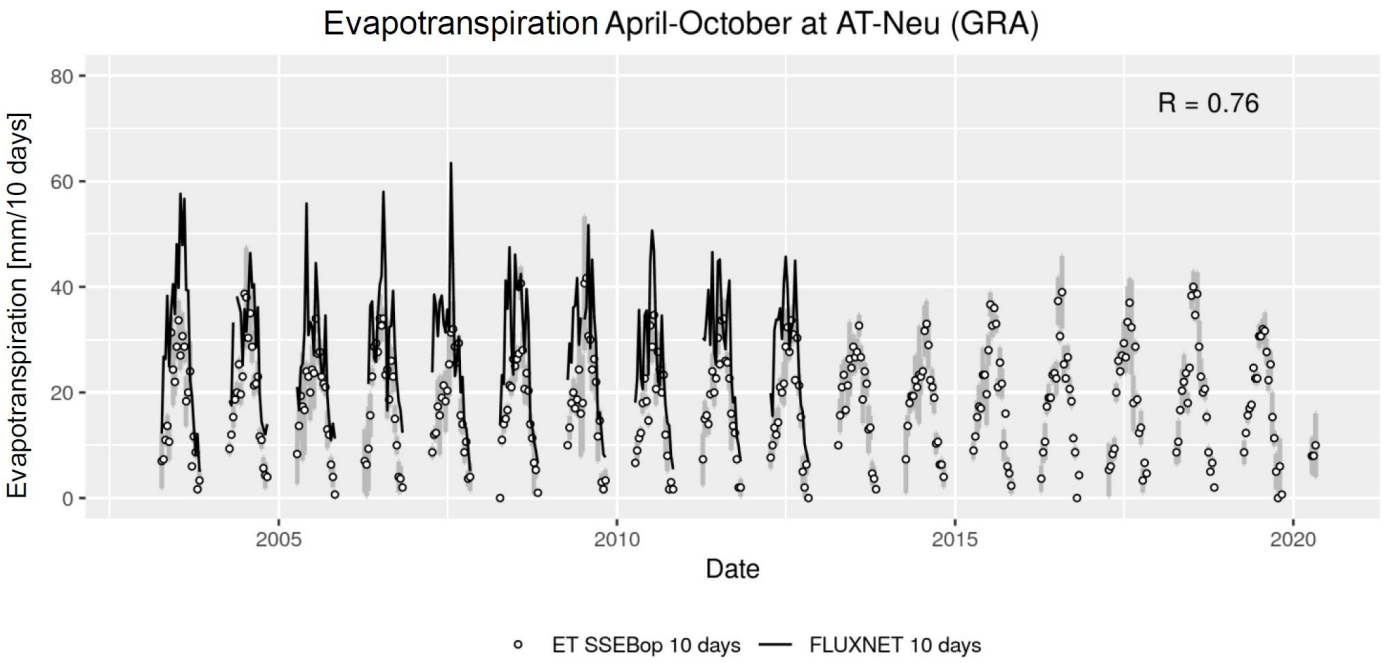

Figure S17. Timeseries of ET from eddy covariance measurements and from the SSEBop product at **the** Fluxnet site AT_Neu.

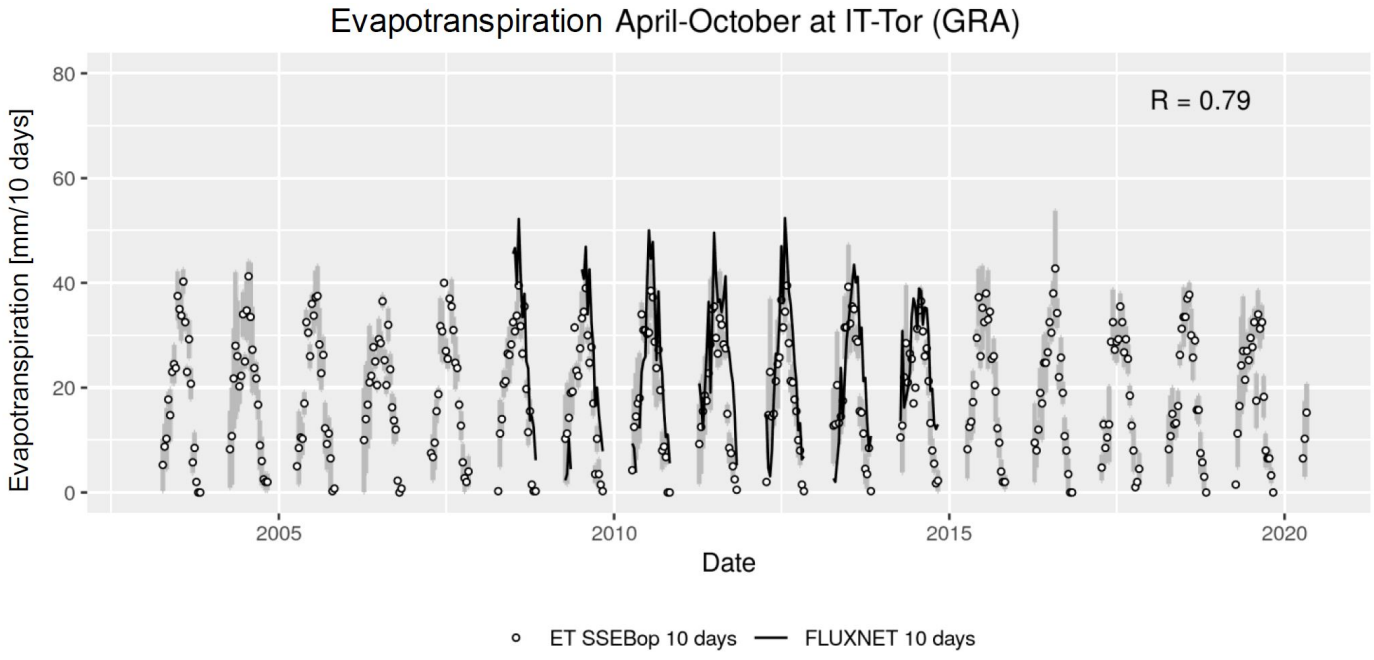

Figure S18. Timeseries of ET from eddy covariance measurements and from the SSEBop product at the Fluxnet site IT-Tor.

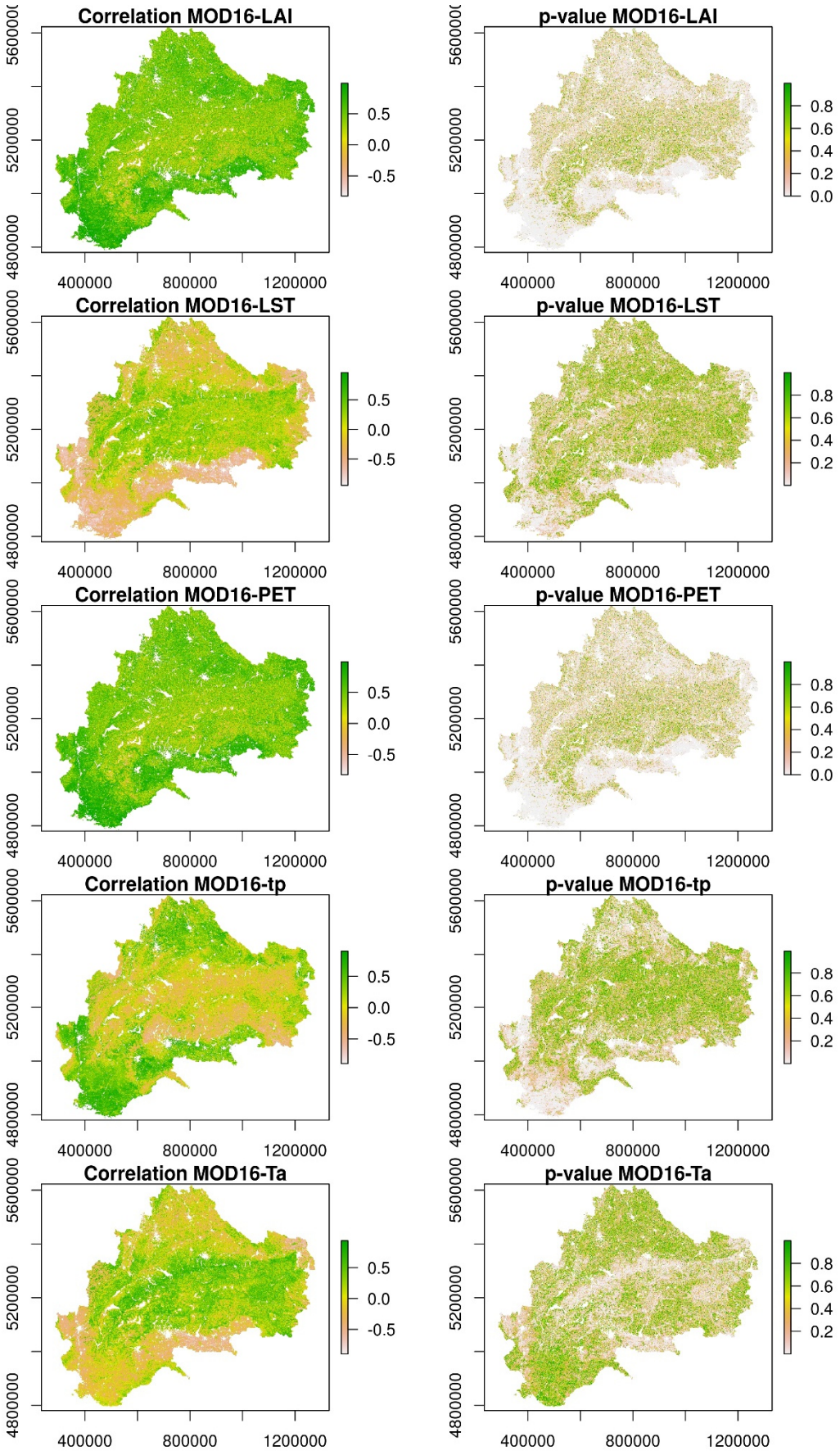

Figure S19: Pixel-wise correlation and *p*-value between MOD16 yearly total ET and LAI, LST, PET, *tp* and *Ta*. LAI (MODIS), **PET** (MODIS) and *tp* (MSWEP) were cumulated over the growing season, while *Ta* (ERA5-Land) and LST (MODIS) were averaged over the growing season.

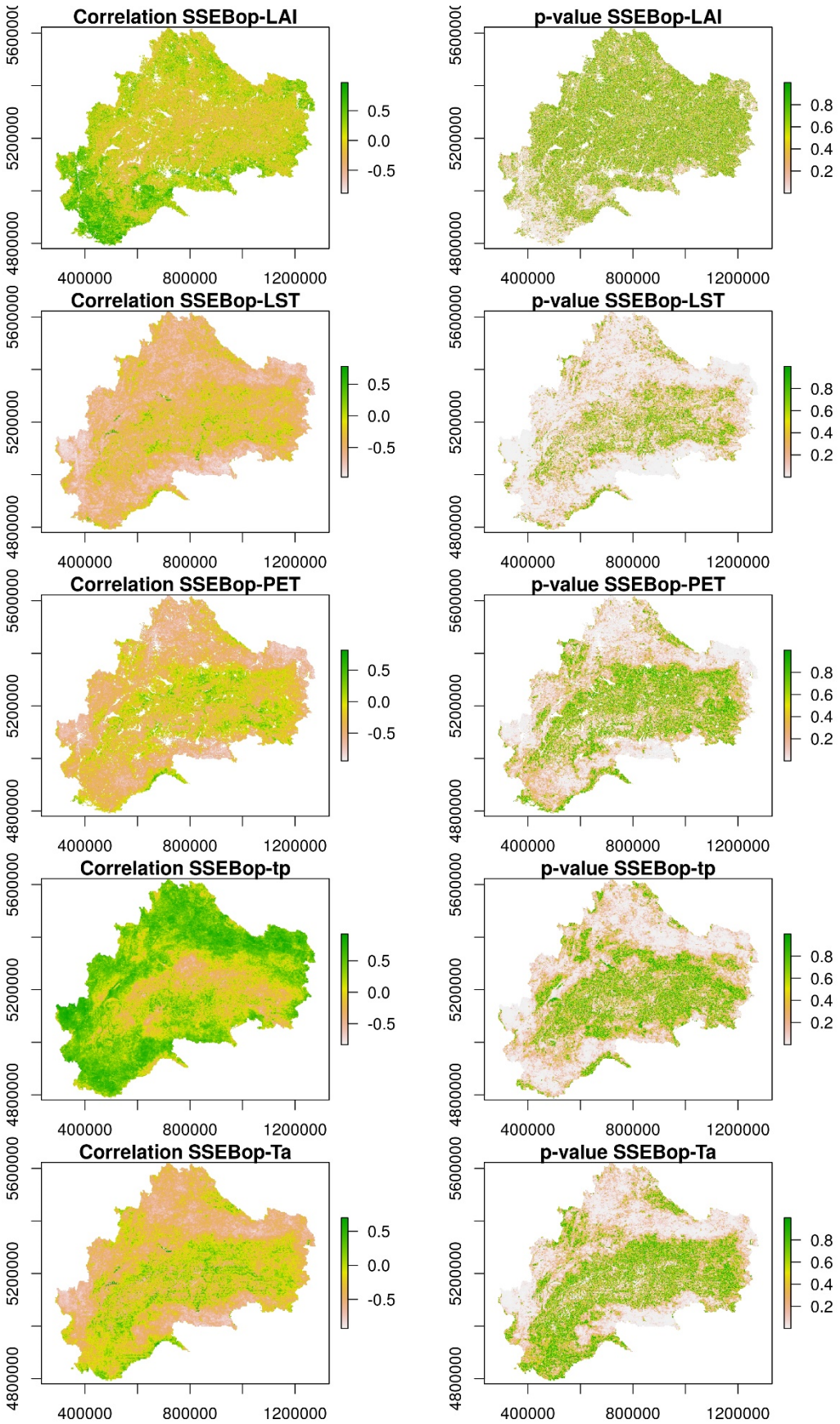

Figure S20. Pixel-wise correlation and *p*-value between SSEBop yearly total ET and LAI, LST, PET, *tp* and *Ta*. LAI (MODIS), PET (MODIS) and *tp* (MSWEP) were cumulated over the growing season, while *Ta* (ERA5-Land) and LST (MODIS) were averaged over the growing season.

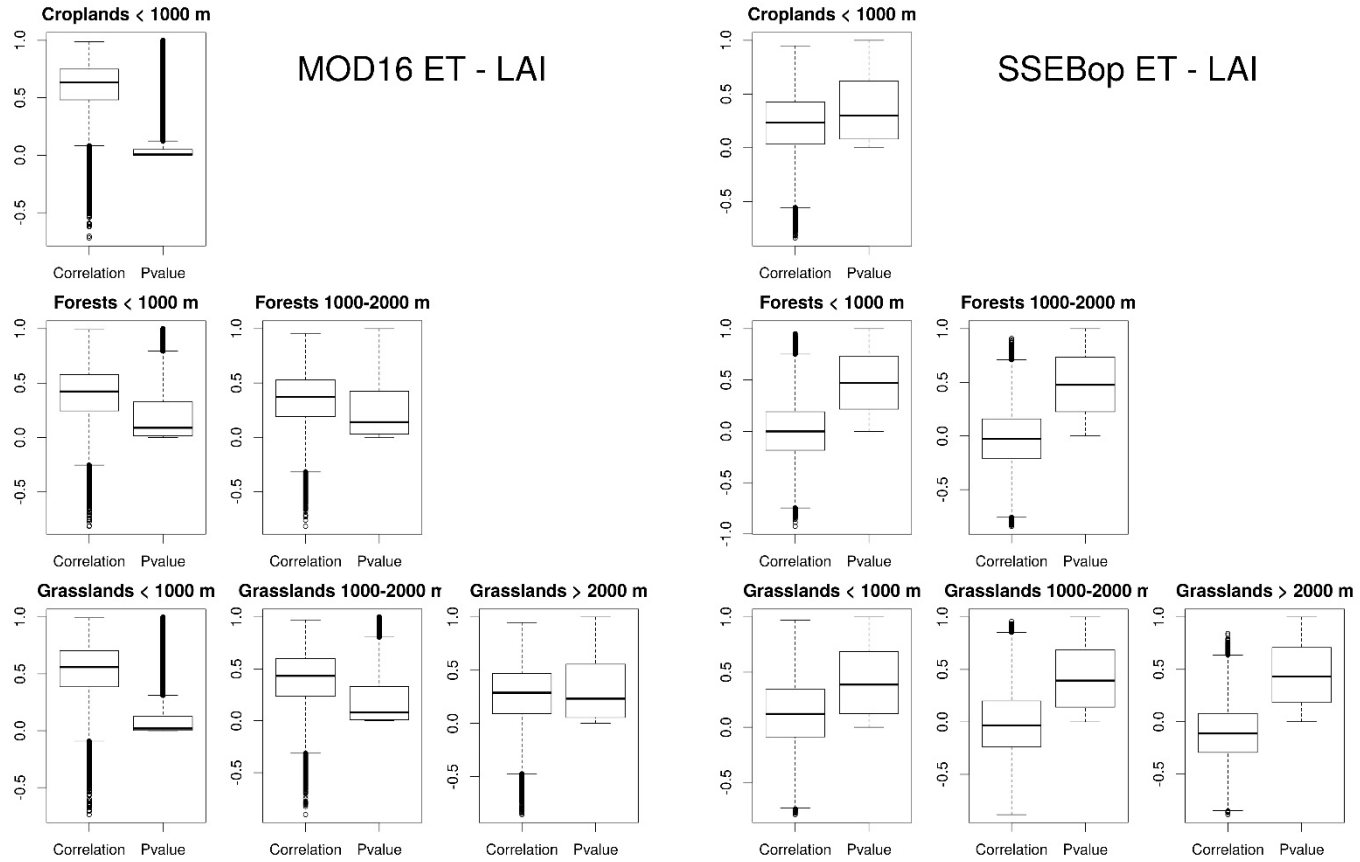

Figure S21. Distribution of the correlation and *p*-value between MOD16 and SSEBop ET and MODIS LAI. All the data were aggregated over the growing season and divided in combined classes of land cover and altitude.

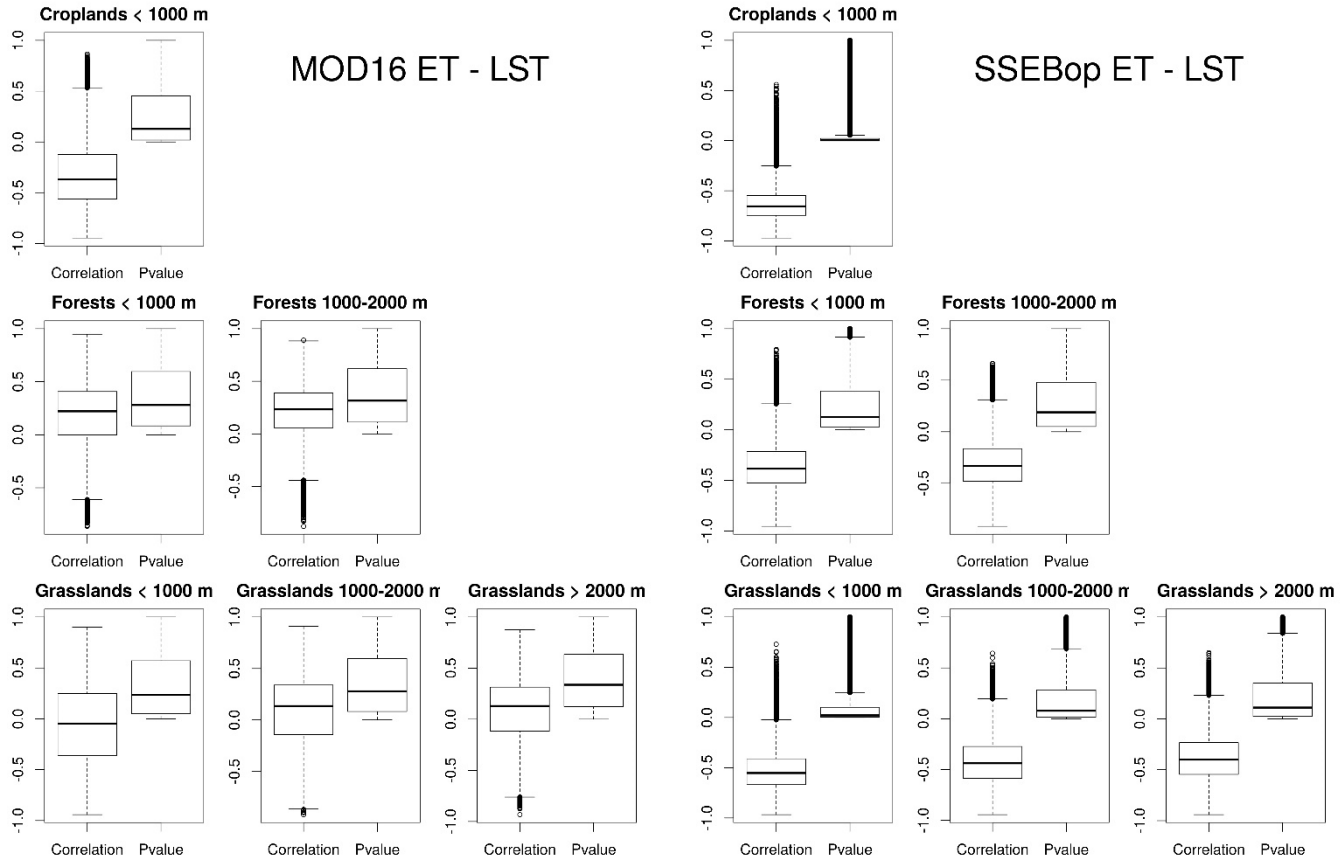

Figure S22: Distribution of the correlation and *p*-value between MOD16 and SSEBop ET and MODIS LST. All the data were aggregated over the growing season and divided in combined classes of land cover and altitude.

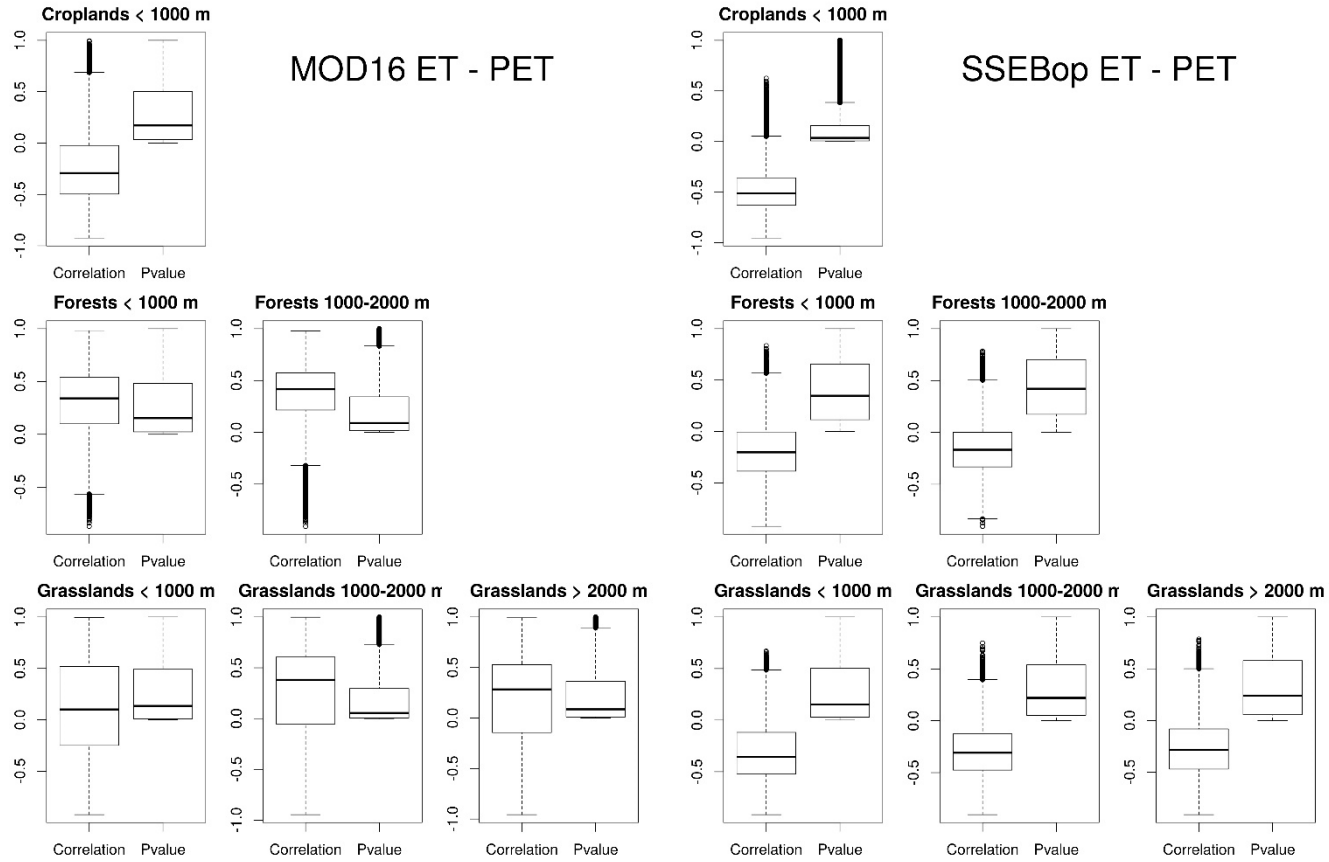

Figure S23. Distribution of the correlation and *p*-value between MOD16 and SSEBop ET and MODIS PET. All the data were aggregated over the growing season and divided in combined classes of land cover and altitude.

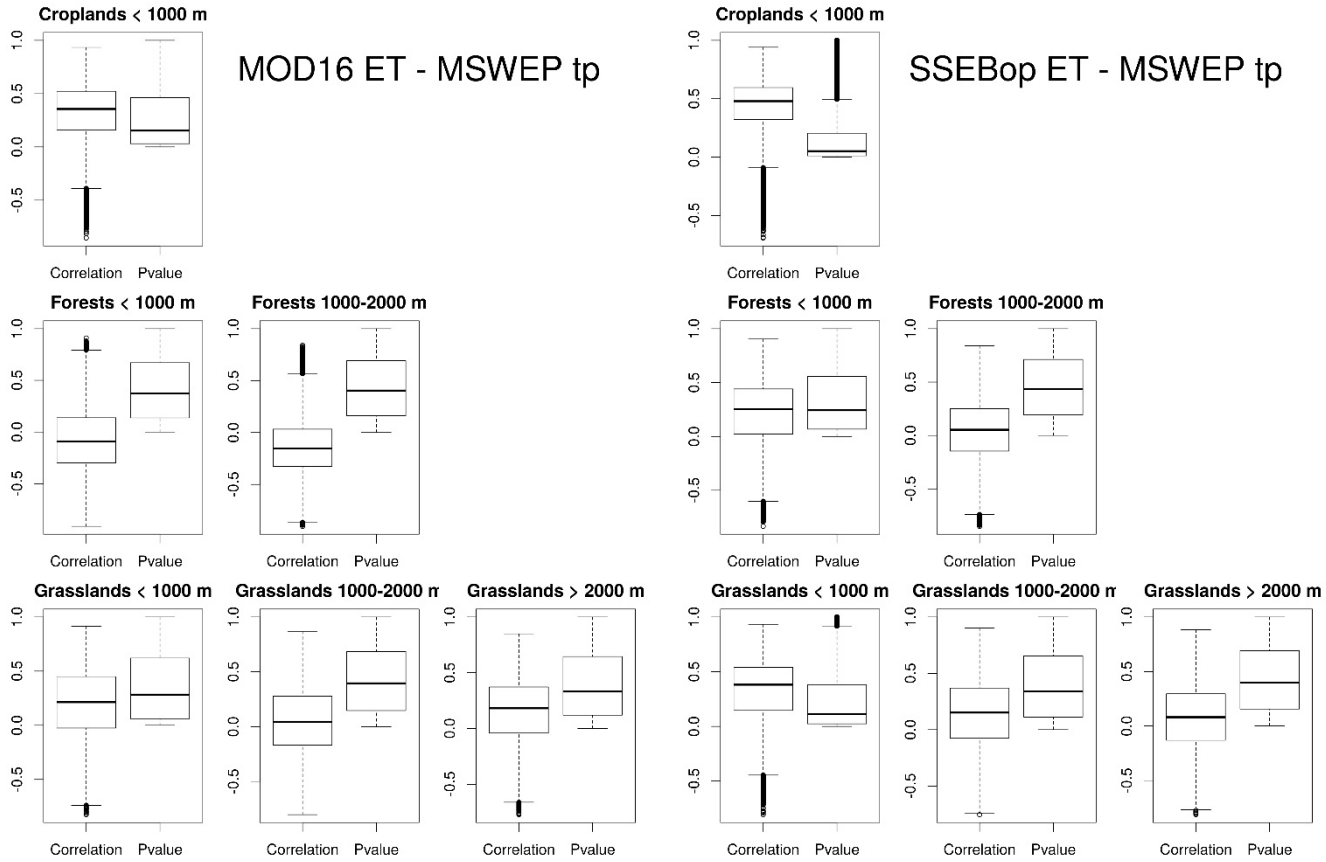

Figure S24. Distribution of the correlation and *p*-value between MOD16 and SSEBop ET and MSWEP precipitation All the data were aggregated over the growing season and divided in combined classes of land cover and altitude.

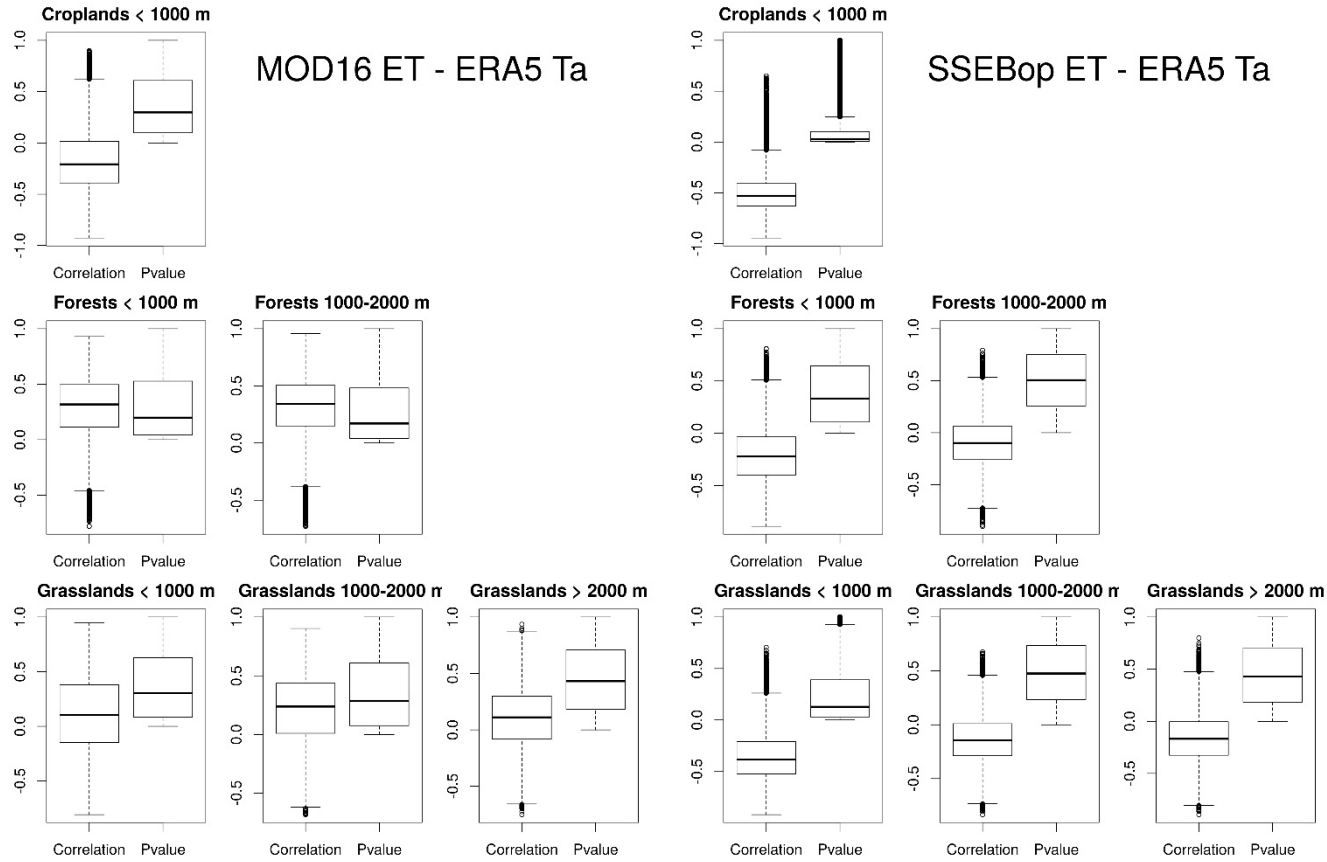

Figure S25. Distribution of the correlation and *p*-value between MOD16 and SSEBop ET and ERA5-Land air temperature. All the data were aggregated over the growing season and divided in combined classes of land cover and altitude.

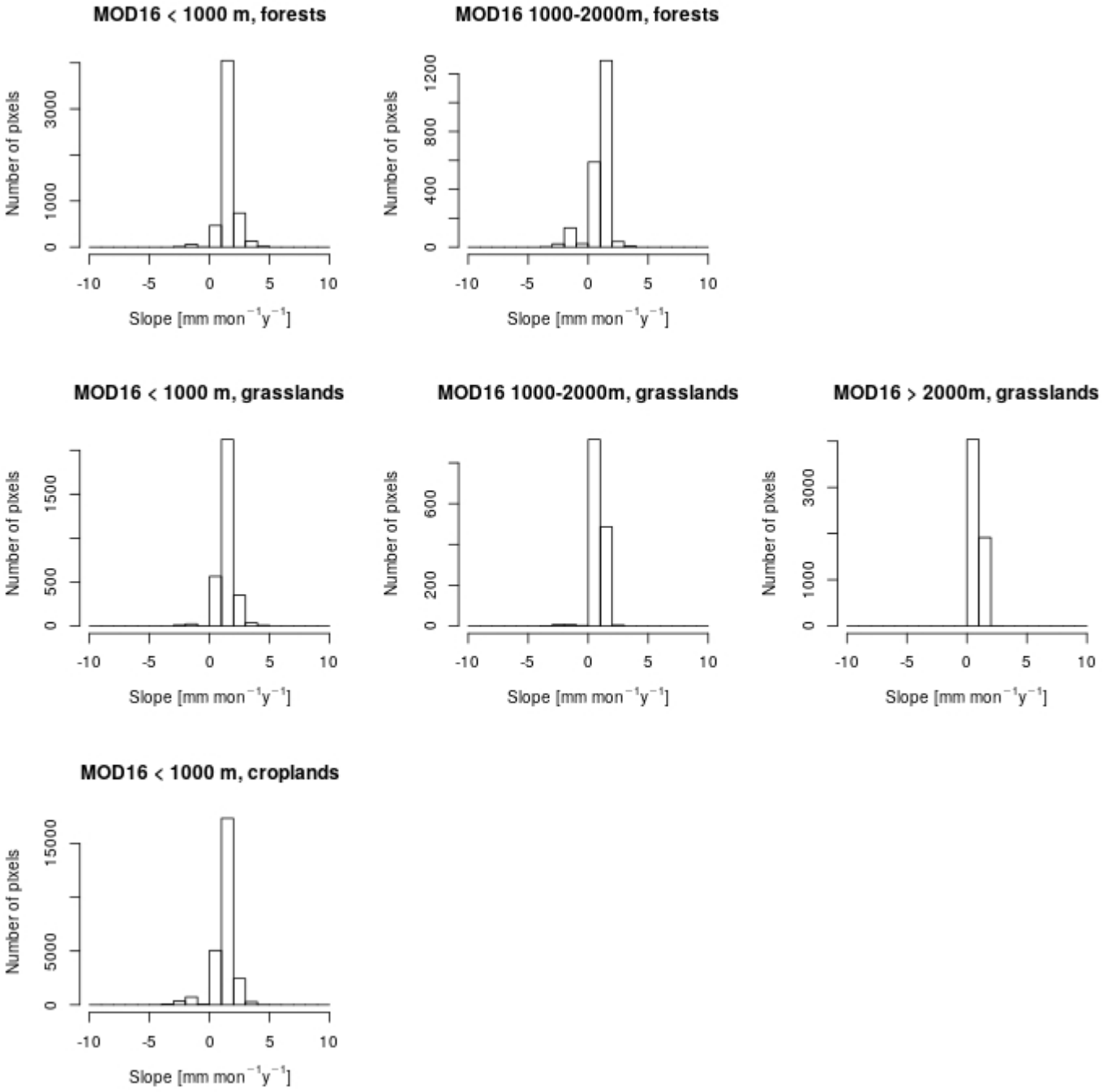

Figure S26. Distribution with elevation and land cover, in number of 500 m x 500 m pixels, of the Sen's slope of the trend of MOD16 monthly ET in May, at 5 % significance level.

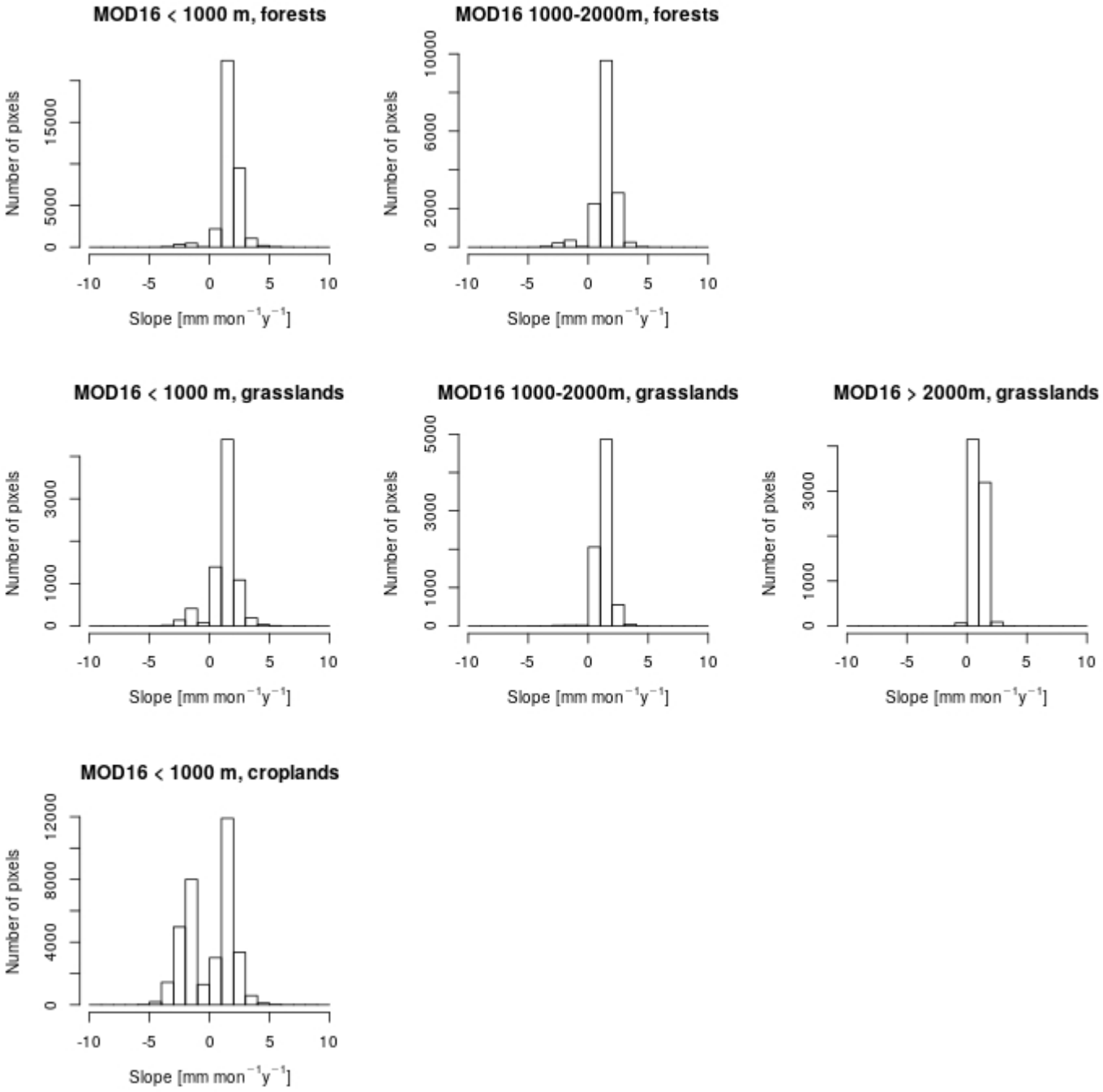

Figure S27. Distribution with elevation and land cover, in number of 500 m x 500 m pixels, of the Sen's slope of the trend of MOD16 monthly ET in June, at 5 % significance level.

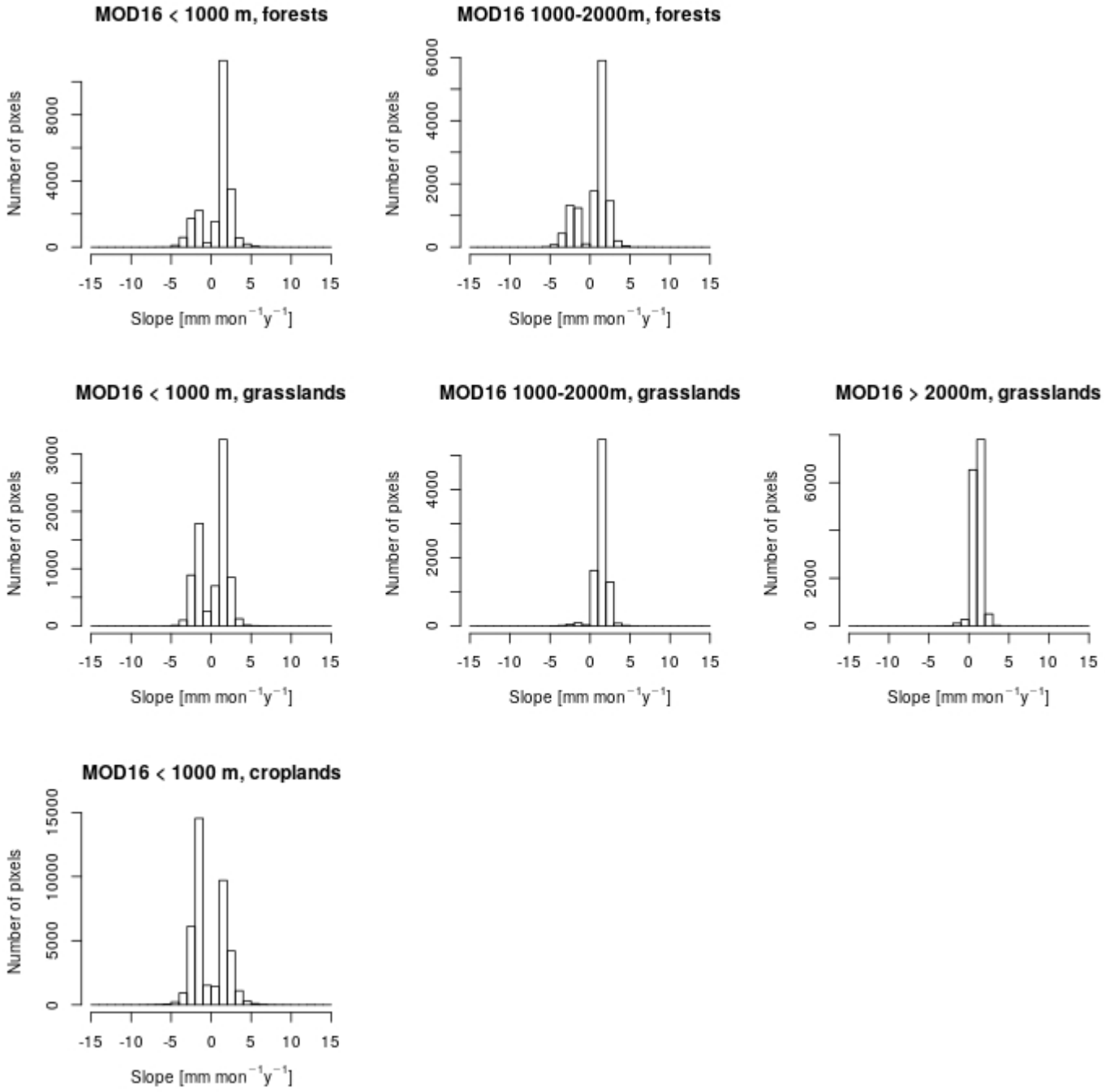

Figure S28. Distribution with elevation and land cover, in number of 500 m x 500 m pixels, of the Sen's slope of the trend of MOD16 monthly ET in July, at 5 % significance level.

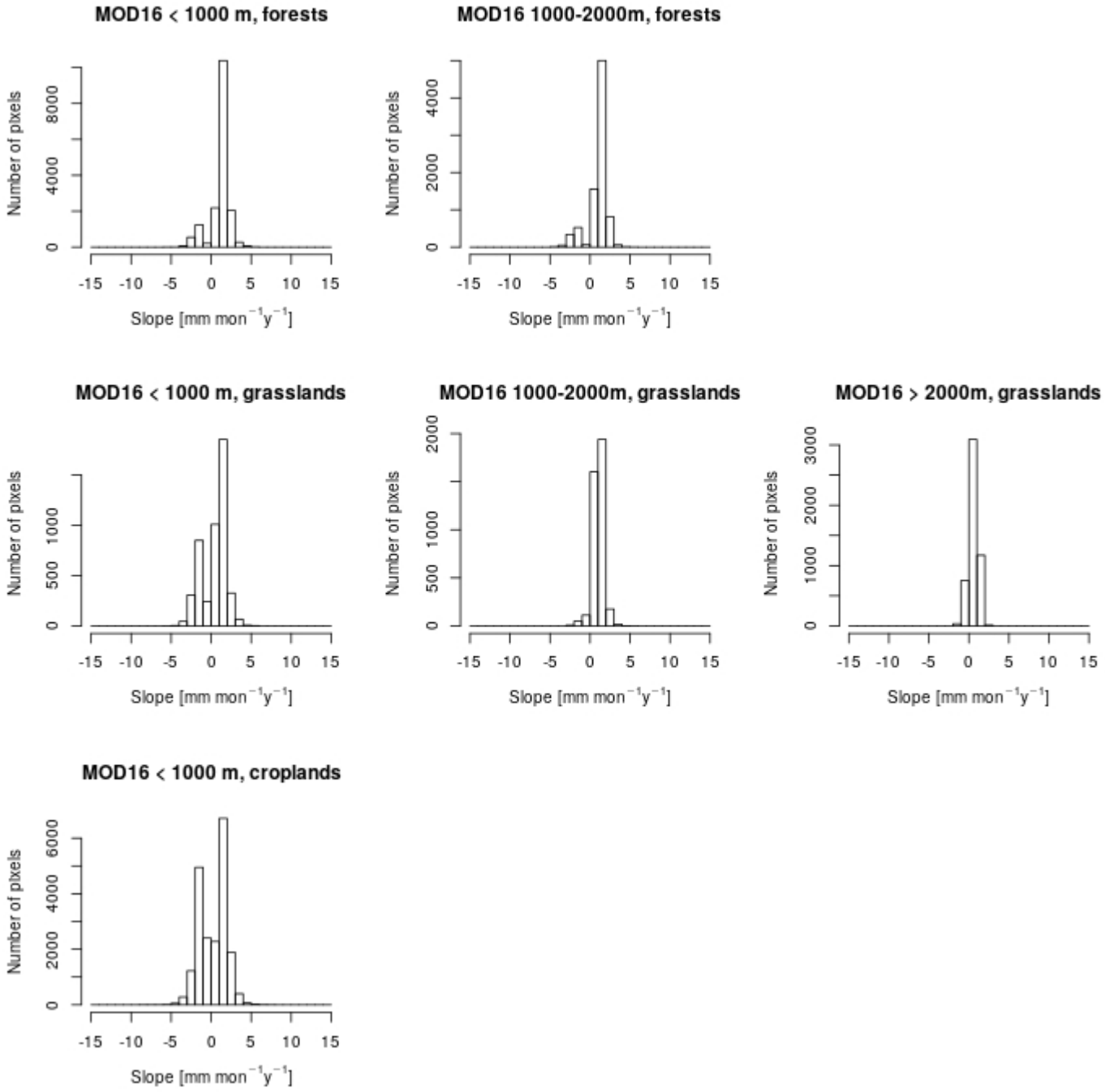

Figure S29. Distribution with elevation and land cover, in number of 500 m x 500 m pixels, of the Sen's slope of the trend of MOD16 monthly ET in August, at 5 % significance level.

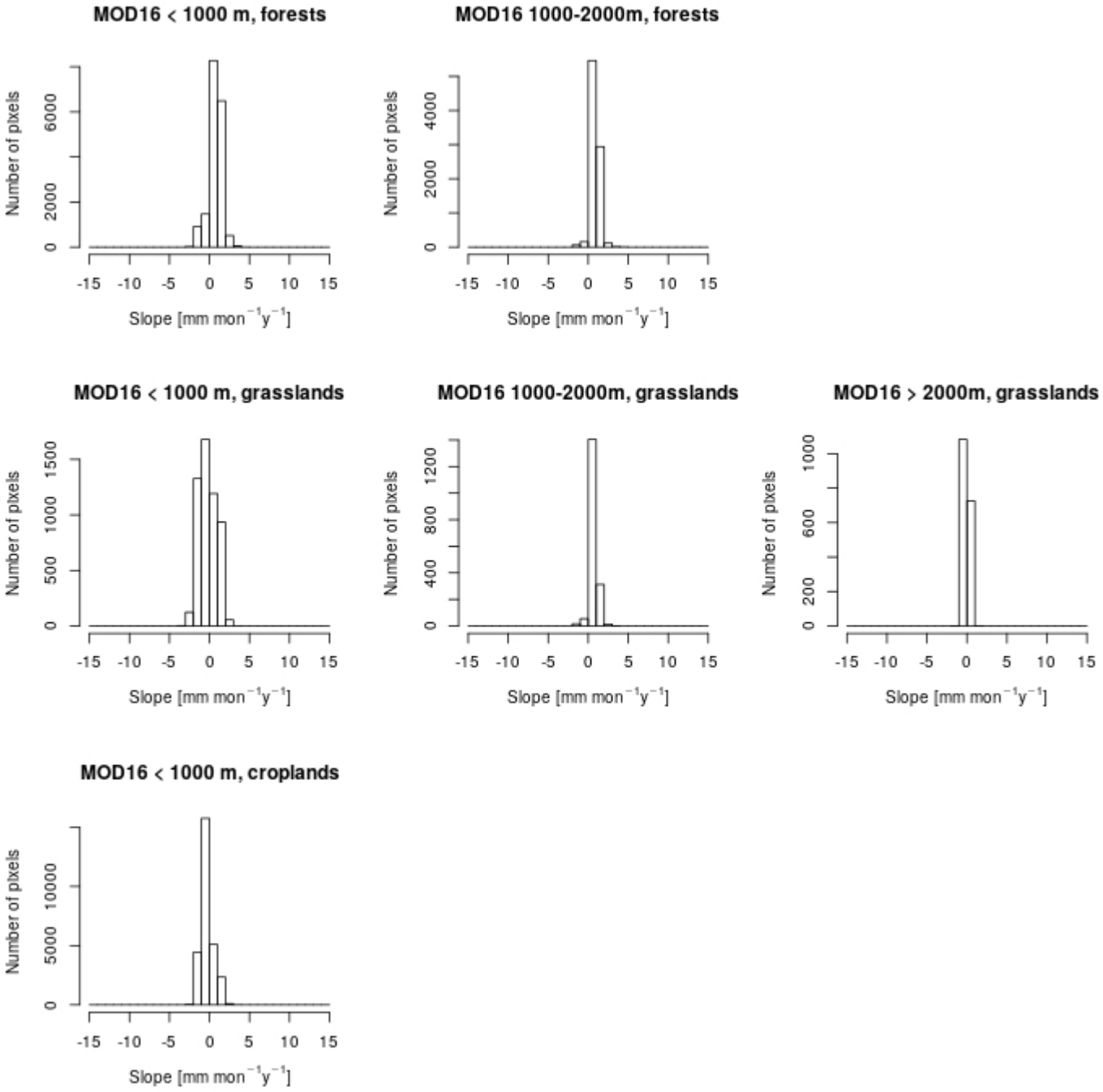

Figure S30. Distribution with elevation and land cover, in number of 500 m x 500 m pixels, of the Sen's slope of the trend of MOD16 monthly ET in September, at 5 % significance level.

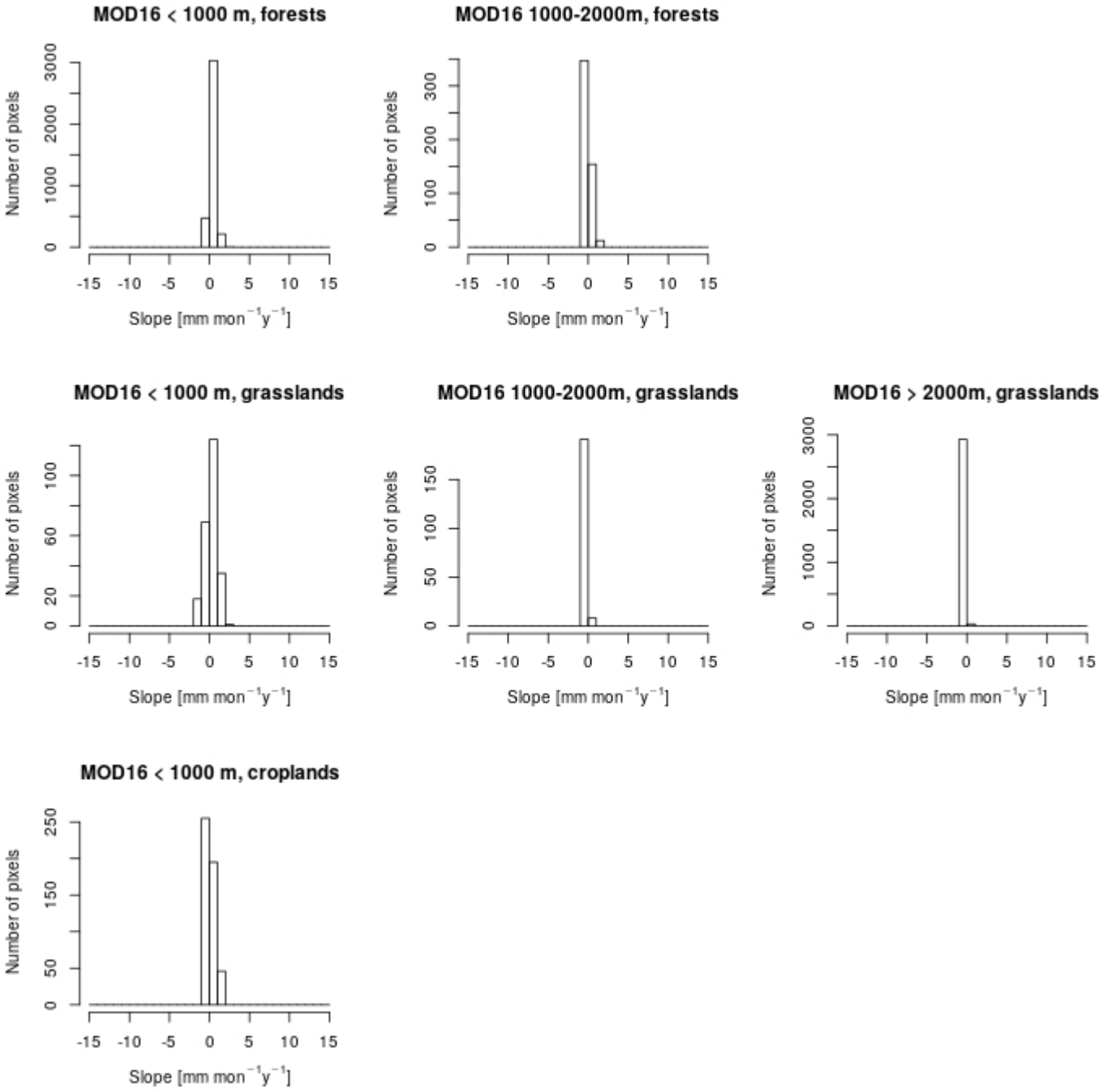

Figure S31. Distribution with elevation and land cover, in number of 500 m x 500 m pixels, of the Sen's slope of the trend of MOD16 monthly ET in October, at 5 % significance level.

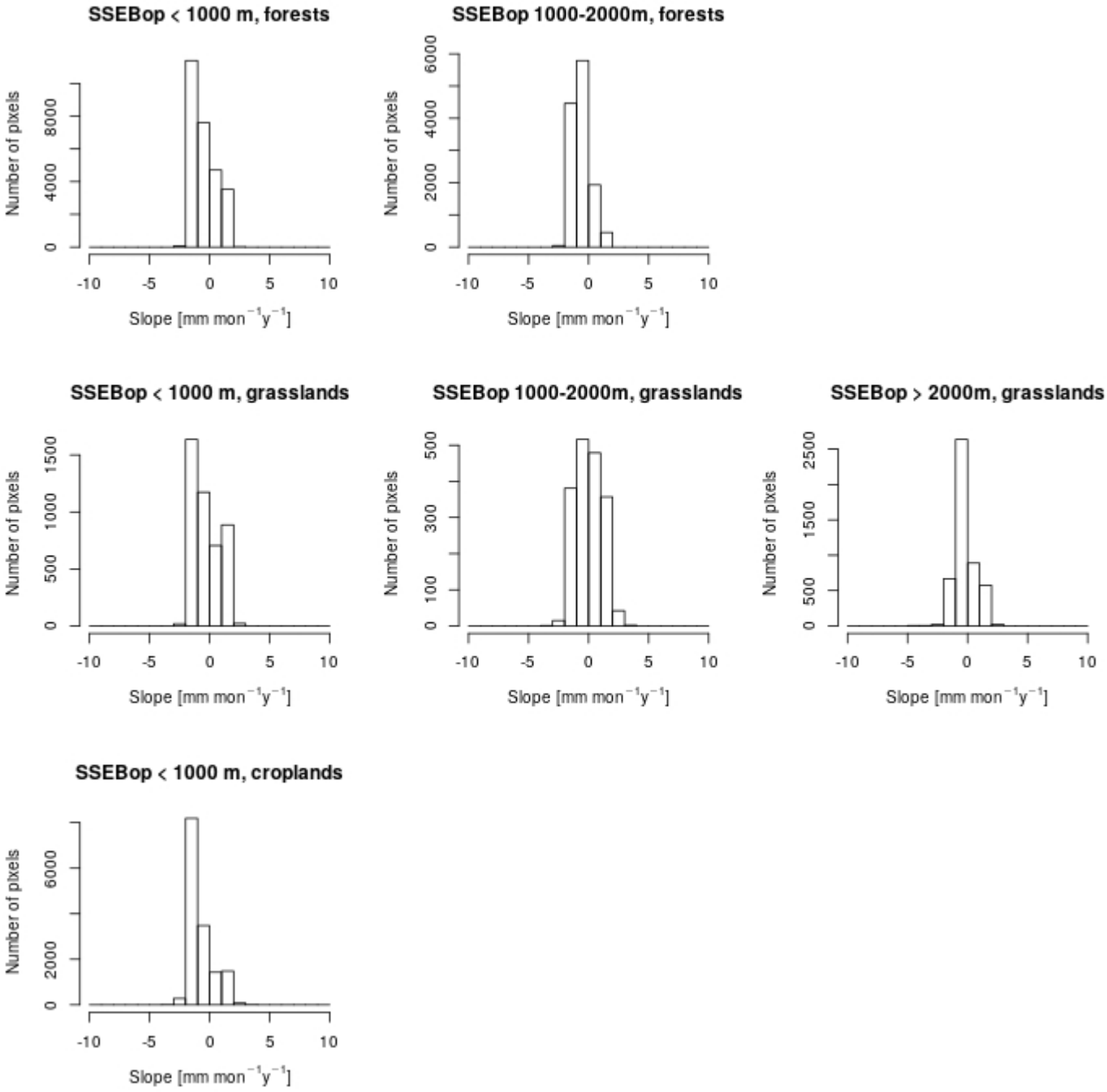

Figure S32. Distribution with elevation and land cover, in number of 500 m x 500 m pixels, of the Sen's slope of the trend of SSEBop monthly ET in April, at 5 % significance level.

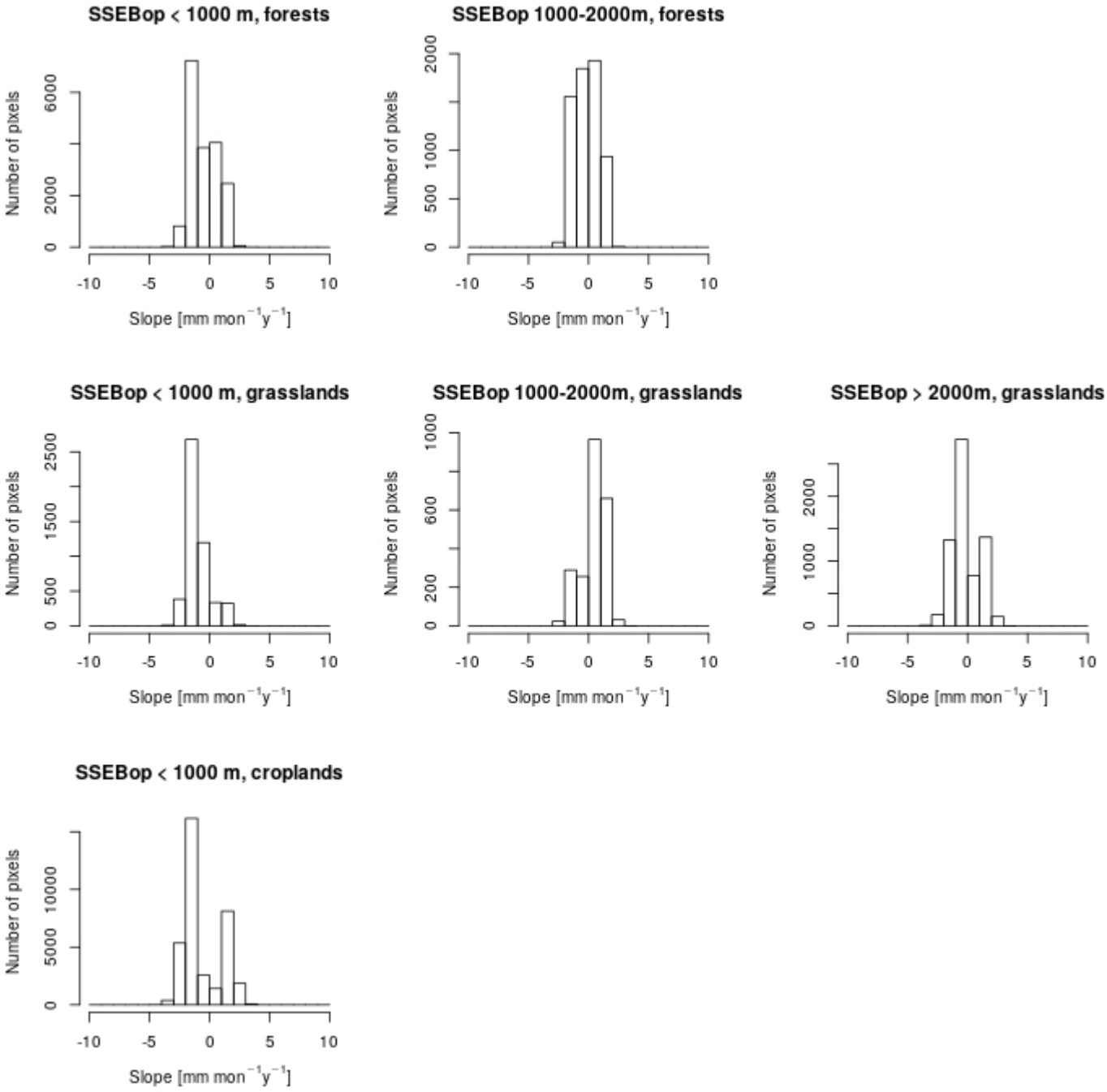

Figure S33. Distribution with elevation and land cover, in number of 500 m x 500 m pixels, of the Sen's slope of the trend of SSEBop monthly ET in May, at 5 % significance level.

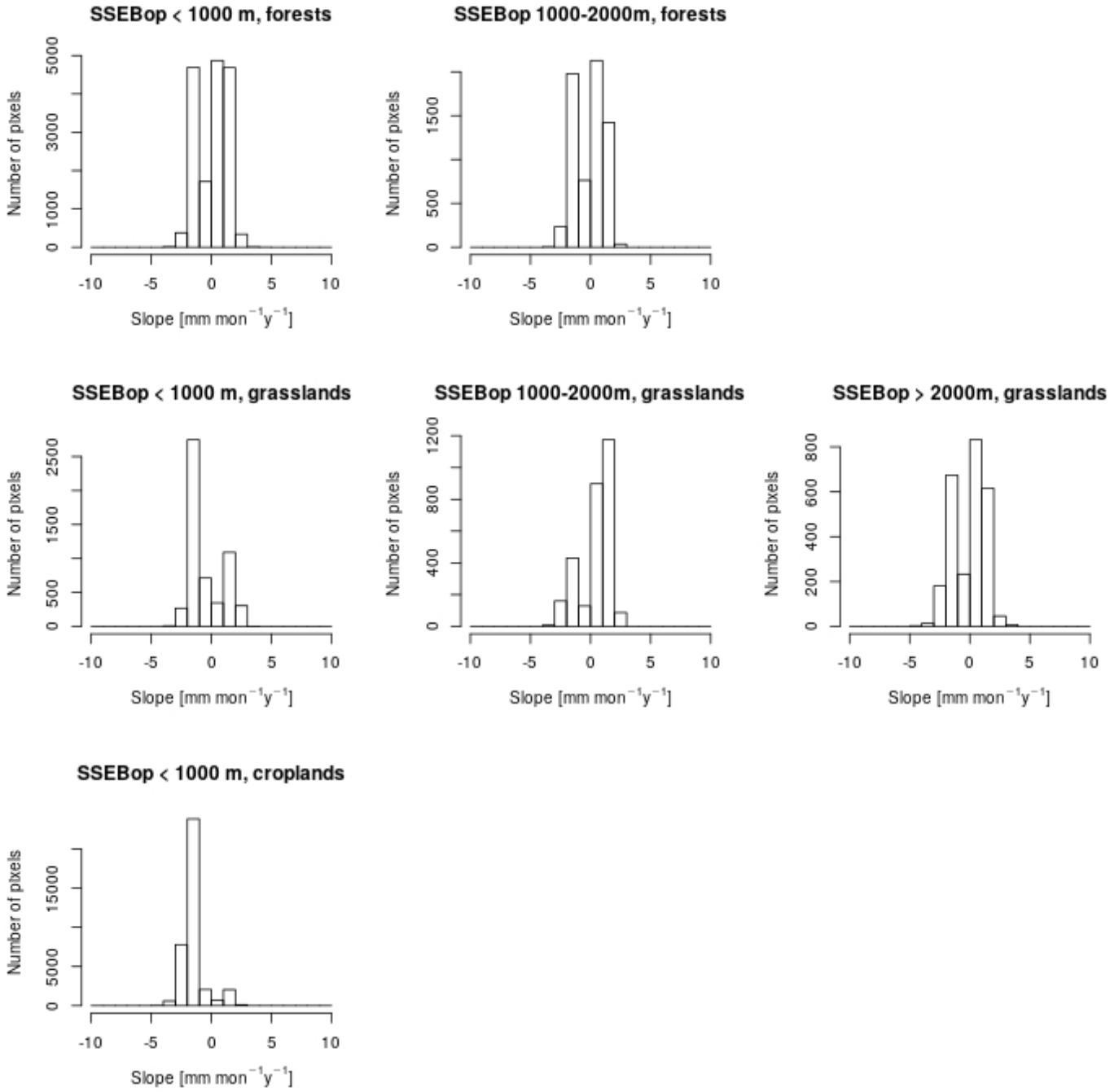

Figure S34. Distribution with elevation and land cover, in number of 500 m x 500 m pixels, of the Sen's slope of the trend of SSEBop monthly ET in June, at 5 % significance level.

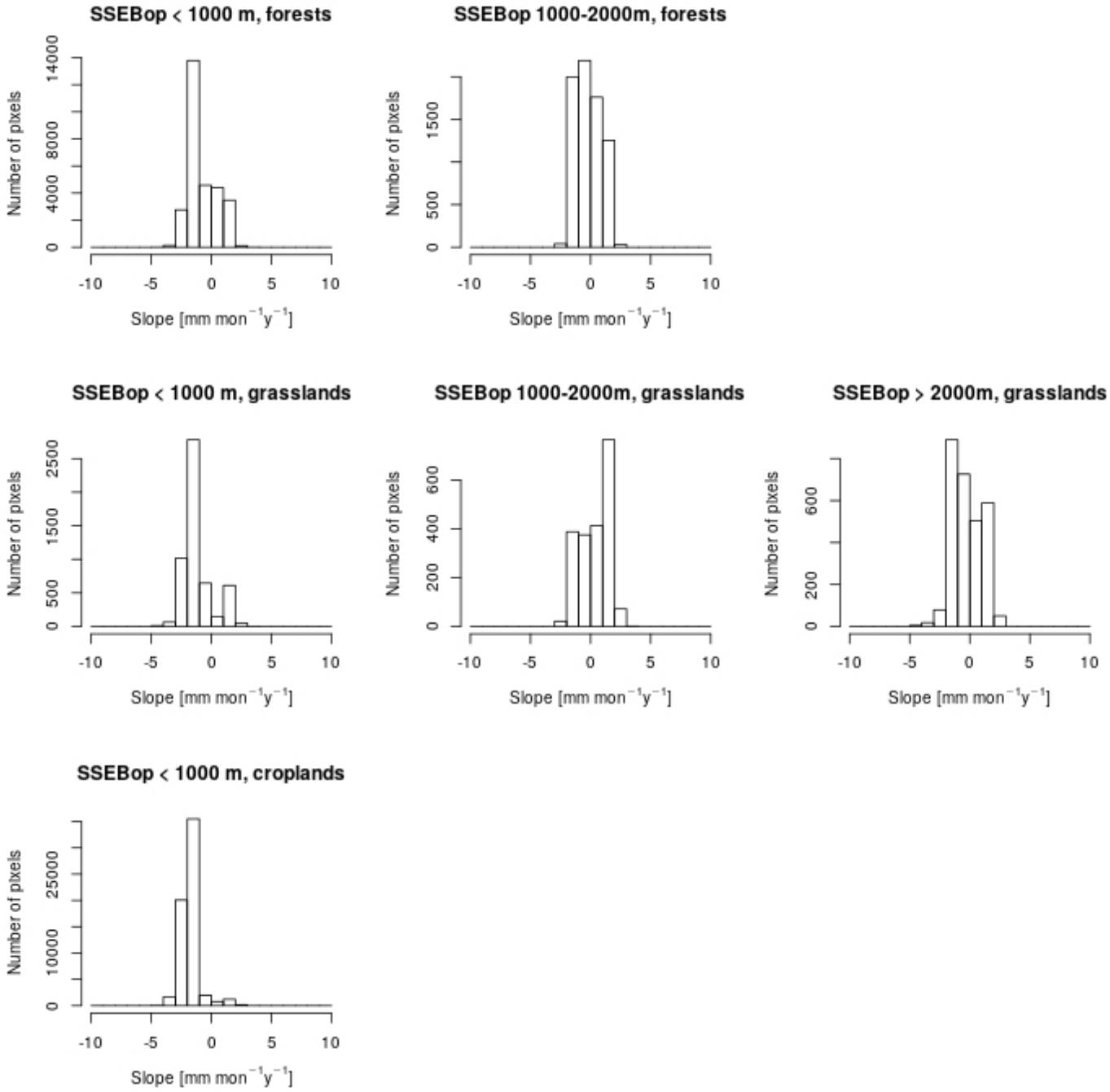

Figure S35. Distribution with elevation and land cover, in number of 500 m x 500 m pixels, of the Sen's slope of the trend of SSEBop monthly ET in July, at 5 % significance level.

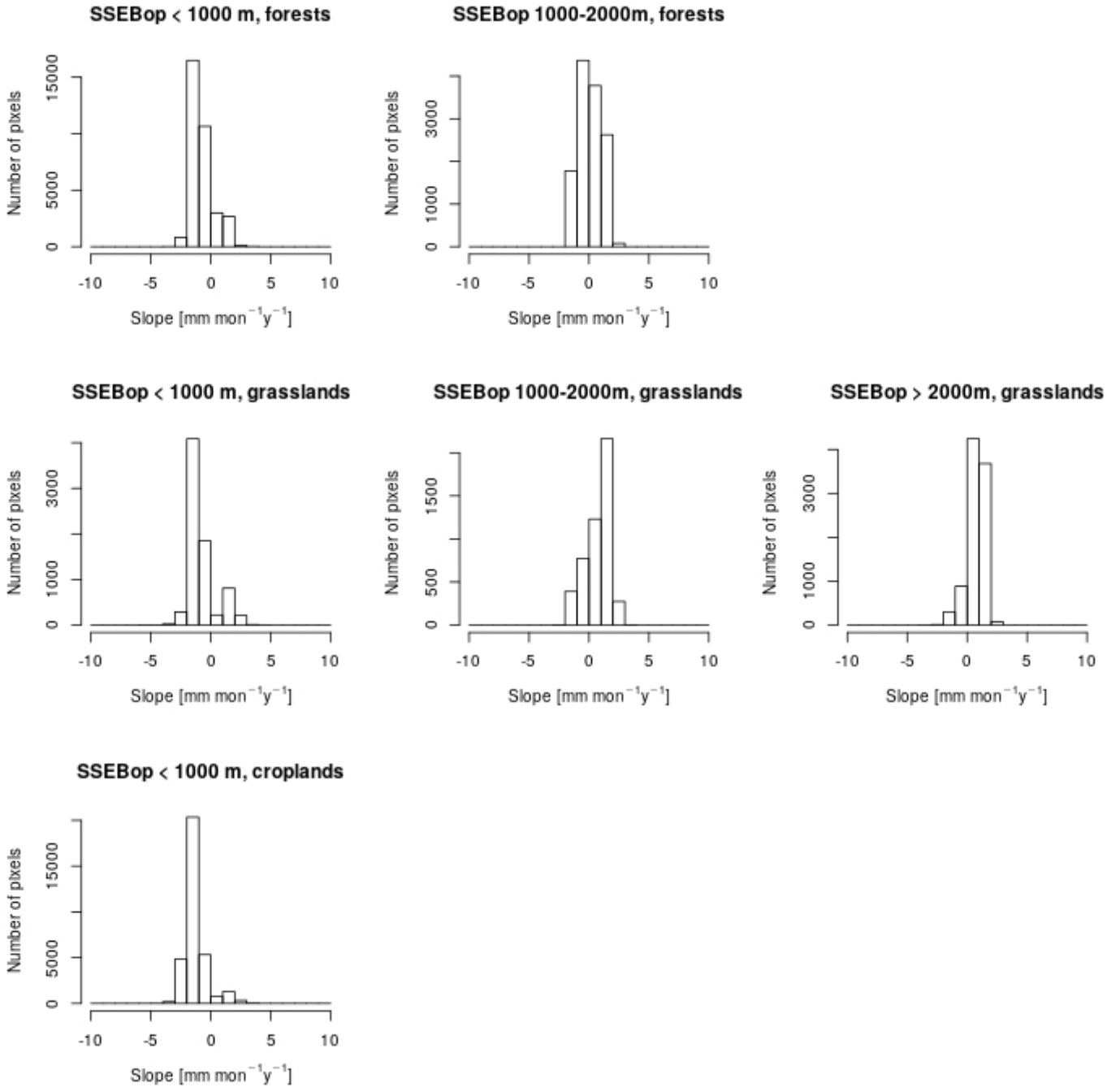

Figure S36. Distribution with elevation and land cover, in number of 500 m x 500 m pixels, of the Sen's slope of the trend of SSEBop monthly ET in August, at 5 % significance level.

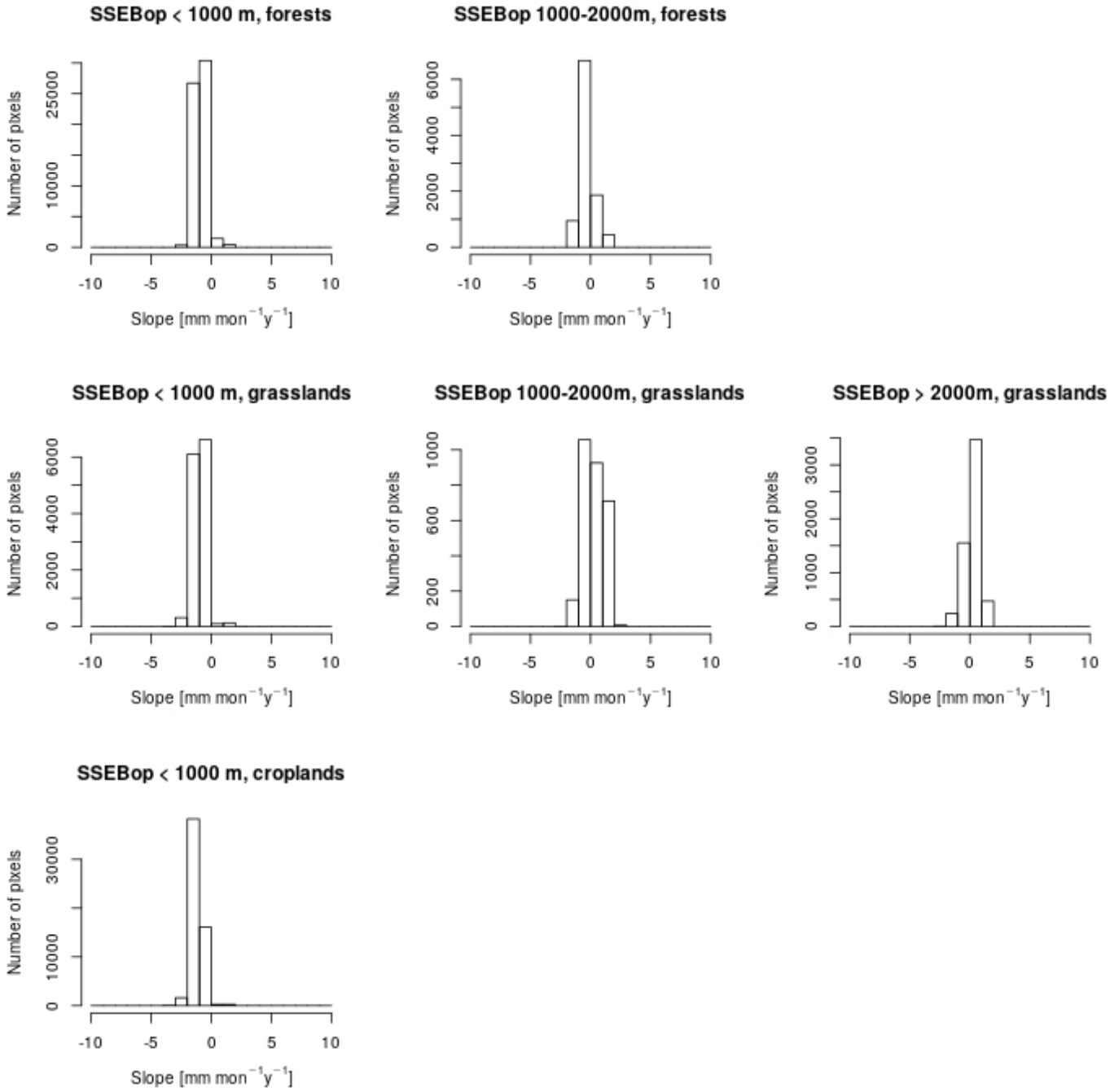

Figure S37. Distribution with elevation and land cover, in number of 500 m x 500 m pixels, of the Sen's slope of the trend of SSEBop monthly ET in September, at 5 % significance level.

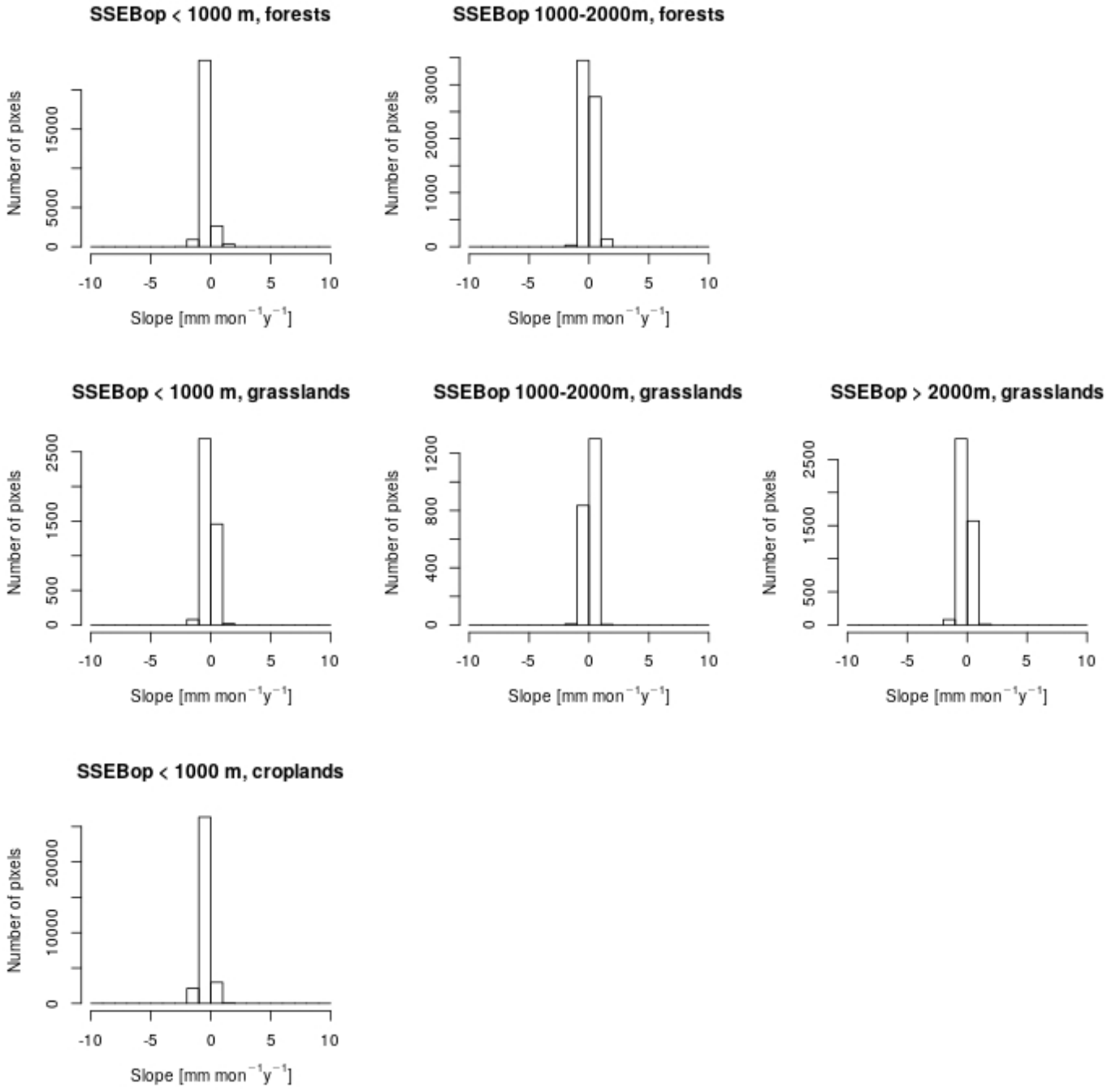

Figure S38. Distribution with elevation and land cover, in number of 500 m x 500 m pixels, of the Sen's slope of the trend of SSEBop monthly ET in October, at 5 % significance level.

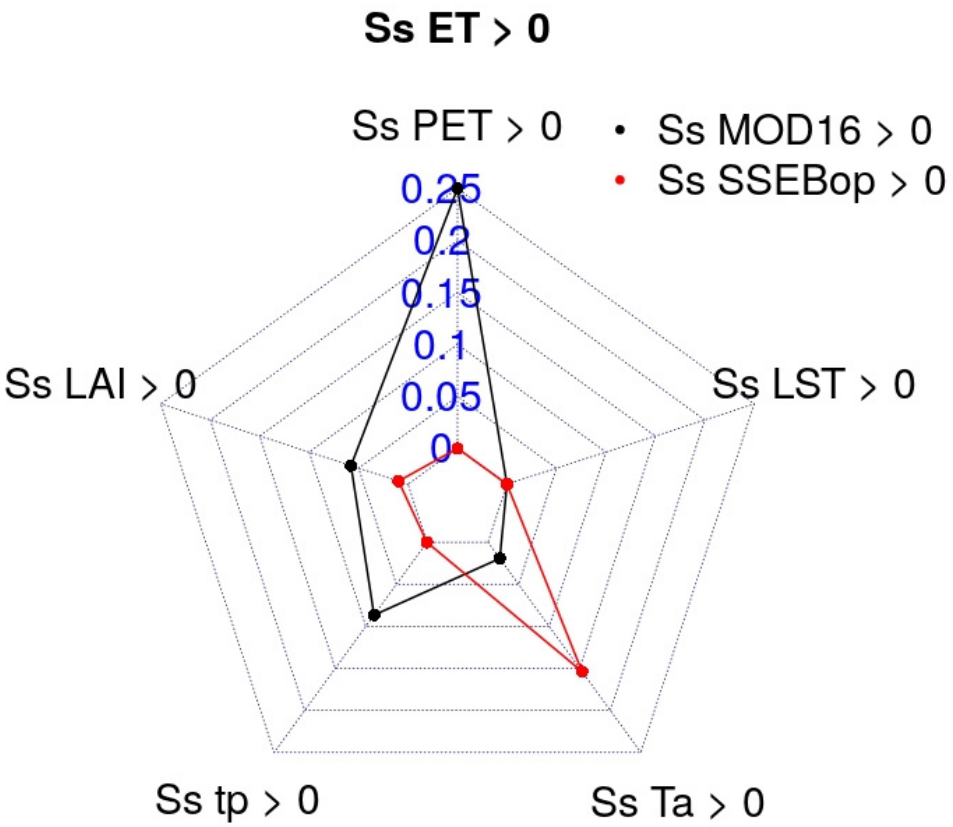

Figure S39. Correlation between positive yearly ET trends and trends in PET, LAI, *tp*, *Ta* and LST.

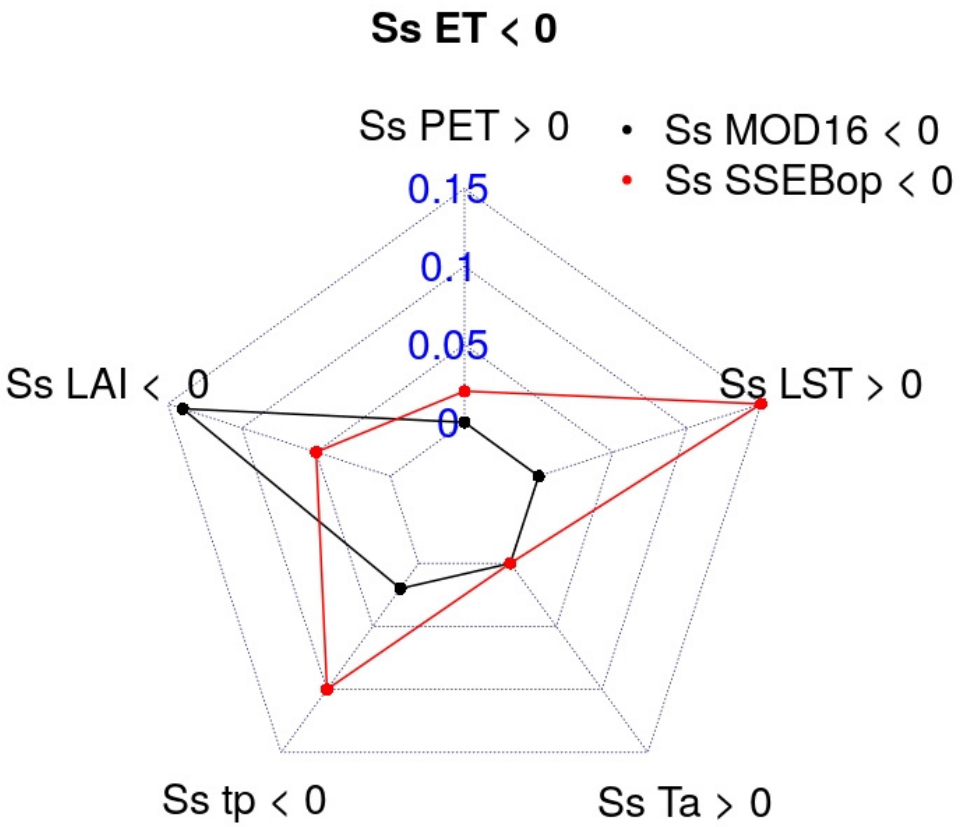

Figure S40. Correlation between negative yearly ET trends and trends in PET, LAI, *tp*, *Ta* and LST.